Rubber Bearing Isolator with Granular and Polymer Filler Core and Application on a Building

Kar Chun Tan[a], Farzad Hejazi[a,*]
[a] *Department of Civil Engineering, University Putra Malaysia, 43400, Selangor, Malaysia*
* Corresponding author. Email: farzad@fhejazi.com

Abstract
In the present study, a new core-and-filler system was proposed to use in elastomer bearings as a substitution to hazardous lead core while improving the performance of base isolators. The proposed system utilizes steel core and filler consists of either granular or polymer materials in relation to this proposal, both pure sand and epoxy are used as filler. Special design procedure for the proposed bearing was developed to determine the required dimension for elastomeric bearing under considered design loads according to the code of practice.
The finite element model of the designed elastomeric bearing was developed to evaluate performance of the proposed bearings under design condition through nonlinear dynamic analysis. Then, parametric study was conducted to simulate various material properties and loading conditions that may occur during the manufacturing and service life of base isolation.
Substantial improvement in performance of proposed bearing with core-and-filler system was observed in comparison to the lead rubber bearing. By reducing the volume of sand filler, the damping bearing of proposed sand and steel core mechanism can be improved. By manipulating the sand packing condition during manufacturing, improvement in term of effective stiffness is achievable. Trilinear constitutive curve for fully sand filled bearing revealed that, the increment in effective stiffness of bearing is higher for the shear strains more than 150%. Therefore, the core-and-filler system with full sand filler provides superior resistance against high shear strain in comparison to the lead-core rubber bearing, and achieve the purpose of limiting lateral displacement.
Application of proposed elastomeric bearings in the 5-story building as base isolator has been proven the effectiveness and suitability of implementing bearing with core and fully filled sand and also with epoxy filler as alternative isolator to the lead core elastomer bearings.
Keywords: Elastomeric bearing, laminated rubber bearing, lead rubber bearing, core and filler system, sand, epoxy resin, finite element method, time history analysis

1.0 Introduction

Base isolation system emerged as one of the most matured seismic protection technologies. The most notable form of such technology is laminated rubber bearing (LRB) [1]. Equipped with alternating rubber layers and reinforcing steel shims, the device not only absorbs the impact, but also achieve structural isolation in the event of ground motion, while dissipate energy at the same time [2][3][4][5].
Efforts have been made on the innovation of base isolator to achieve greater improvement. Among those innovation, lead-core rubber bearing (LCRB) introduced by Robinson in year 1982 brought significant influence on the technology. Utilizing the recrystallization of lead in room temperature and its low yield strength i.e. 10MPa, continuous yielding and restoring process is exploited and this grants the LCRB superior damping. The addition of lead simply improves the stiffness of elastomeric bearing too [6][7]. Another notable bearing in research is fibre-reinforced rubber bearing (FRRB), introduced as early as year 1992. Rather than using steel plates, FRRB uses fibre reinforcement material (FRP) and significantly reduces the weight of bearing and manufacturing cost. The resistance of FRRB is provided through contact friction between FRP and rubber layers [8]. FRRB is compatible with recycled rubber and this reduces its manufacturing cost. The inferiority of recycled rubber in terms of the mechanical properties

is overcame by using unbonded configuration, where the bearing is allowed to roll off under shear, and thus avoid the production of high tensile stress in rubber layers [9].
Matsushita, Fujisaki and Sasaki proposed peripherally restrained bearing (PRB), which added a synthetic rubber core to LRB [10]. Other than using FRP, Li et al. explored the feasibility of replacing steel shims in a conventional rubber bearing with steel mesh [11]. In some studies, shape memory alloy is introduced to bearing as external bracing, and the improvement has been proven satisfying [12][13].
Tan et al. proposed core-and-filler mechanism as an improvement to the conventional elastomeric bearing. The implementation of steel core and filler has been proven effective in improving the shear strength and energy dissipation of bearing, while bringing reduction in terms of damping. The researchers remarked that system with fully filled sand is the most favourable mechanism as the improvement achieved was the highest, while the decline in damping is insignificant [14].
Among the discussed base isolator variations, both LRB and LCRB has significantly high implementation compared to others. Alongside the wide implementation, major drawbacks were identified. For LRB, there is no mean for the device to control the lateral displacement, instead the dimension and specification of bearing is designed based on the estimated force and allowable displacement. In the event of unpredictable scenario, large force may be applied and causes the device to deform largely. When subjected to large strain, rubber hardening occurs, and the device begins to lose its flexibility. As a result, the isolation capability of device deteriorates, and this allows greater amount of force to be transferred to superstructure. The structure might be at risk with these extra forces that are not foreseen during the design stage [11][15]. When elastomeric bearing performance deteriorates, large deformation happens, and the structure might face global stability problem. Unseating failure occurs and consequently, the structure may collapse or topple over [16]. The drawbacks of the LCRB are on the sustainability aspect. Lead is proven a hazardous material that brings soil contamination that may persist for centuries [17][18]. Lands that involved in lead-related purpose such as mining, manufacturing, and recycling are harmful to the health of people reside in it or nearby it without proper mitigation [19][20].
There are several factors that influence the performance of an elastomeric bearing. The most notable effect is the geometry of elastomer in use. It is usually described using secondary shape factor S_2, which is the ratio of elastomer's plan width to thickness [21][22]. The shape factor governs the failure mode of bearing under compression and shear. For stocky bearing where S_2 is greater than 2.5 to 3, the failure of bearing is governed by shear. On the other hand, the failure mode of slender bearing with S_2 less than 2.5 is governed by buckling [22][23].
For LCRB, the factor that mainly influence the performance of bearing is lead core instead of rubber. The larger the diameter of lead core, the greater the stiffness of LCRB. Other than geometry of lead core, the performance of LCRB is also affected by temperature, loading history and aging condition [24][25]. Similar to LCRB, the performance of PRB is also dependent of rubber core, especially in terms of damping [26].
For FRRB, restraint condition governs the behaviour of bearing. When FRRB is fully bonded, where steel plates present at the top and bottom of bearing, the shear stiffness of bearing is superior to the unbonded variant [27][28]. Unbonded FEEB usually rollover and exhibit rotational deformation upon lateral loading [29]. Other than that, the performance of FRRB is also influenced by its geometry [30].
Loading conditions were identified as another group of influencing factors for elastomeric bearing. Among them, exerted compression, shear strain and loading frequency are some of the most notable factors [11].
The study of the behavior of elastomeric bearing, and relevant parametric study can be performed using finite element modeling, although recent phenomenological approaches can

be employed to drastically reduce the computational times without affecting the results accuracy [31][32][26]. Challenges were encountered when modelling the constituent material, rubber. Modelling of rubber material is usually conducted by using hyperelastic constitutive models with experimental result for uniaxial, biaxial and planar extension tests [33]. Several researchers provided sets of test result, such as Treloar (1944), Rivlin and Saunders (1951), Jones and Treloar (1975), Vangerko and Treloar (1978) [34][35][36][37]. These results are often treated as classical experimental result. On the other hand, several studies were conducted to develop hyperelastic constitutive model and attempt to fit the classical experimental results with those models. Some of these notable models are developed by: Ogden (1972), Arruda & Boyce (1993) and Caroll (2011) [38][39][40].

The effectiveness of hyperelastic models was inspected through numerical analysis of elastomeric bearings. Simple model such as neo-Hookean model was remarked as unreliable when large lateral displacement was applied to the simulated bearing, and this is mostly due to the neglection of rubber stiffening that takes place when large shear strain occurs [41]. In other words, the model is deemed reliable when small strain is applied, which caused the rubber to stretch with ratio of 1.5 or less [42]. For other hyperelastic models, it is worth noting that Mooney-Rivlin model faces same issue with the neo-Hookean model, in terms of its deficiency in simulating the stiffening of rubber due to huge shear deformation [43]. Kalfas, Mitoulis & Katakalos on the other hand, concluded that Ogden model produces accurate simulation of the behaviour of natural rubber [44].

Modelling of granular material is commonly conducted using discrete element modelling (DEM) This method was introduced by Cundall and Strack [45], and it is usually implemented in research simulating the sand behaviour under various strength tests [46][47]. The major drawback of discrete element modelling is computational cost, where long analysis runtime is required [48][49][50]. Alternatively, the mass of granular material may be modelled as continuum. In relation to that, the sand behaviour can be described by using model considering only elasticity, such as general elastic or porous elastic. More sophisticated models such as Mohr-Coulomb and Drucker Prager are added on to simulate the plastic behaviour of sand mass [51].

In the present study, a new rubber elastomer bearing with steel core and filler system consists of granular or polymer filler is developed as an alternative system to lead core bearing isolators. The pure sand is implemented as granular filler and epoxy is used as polymer filler. The performance of proposed elastomeric bearings was assessed by comparing its performance with lead rubber bearing through finite element simulation. Then, a design workflow for elastomeric bearing equipped with core-and-filler system that complies with the referred design standard is proposed to determine required dimension of bearing components based on considered design loads.

Thereafter, the parametric study is performed to determine the hysteresis behaviour of proposed elastomeric bearings under various material properties and loading conditions. Subsequently, the application of elastomeric bearing with the proposed core-and-filler mechanism in a 5-story structure is simulated and the structural response under applied ground motion is studied and compared with the fixed base structure.

2.0 Development of Elastomeric Bearing with Granular and Polymer Filler Mechanism

In this study, a new elastomeric rubber bearing with steel tube core, alongside both granular and polymer filler mechanism has been developed as an alternative to lead core bearings which nowadays considered as toxic material.

The filler is the primary contributor to the stiffness and energy dissipation of elastomeric bearing. Two types of mechanisms are used as filler in the proposed bearings:

i. The first mechanism seeks resistance from filler mass through friction between interlocking granulates. This mechanism requires the filler to be made of granular material i.e. pure sand. The addition of large particle such as gravel has been proven bringing insignificant improvement to the shear strength of sand mixture, and without gravel the abrasivity of contacting components can be minimized [52][53][54].
ii. The second mechanism adopts epoxy resin, a type of polymer that is commonly implemented in construction industry such as pavement engineering, where the binder mixed with epoxy resin has greater resilience compared to untreated samples [55][56].

The steel core is added to strengthen the filler in the proposed elastomeric rubber bearing. A gap is presented between the steel core and the interior of elastomeric bearing body. When the bearing is subjected to large stroke and causes the contact between steel core and bearing body, the resistance of steel core is deployed. This makes further stroke harder to achieve without adding more force. Fig. 1 shows the proposed elastomeric bearing equipped with core-and-filler system, and its behaviour under different situations.

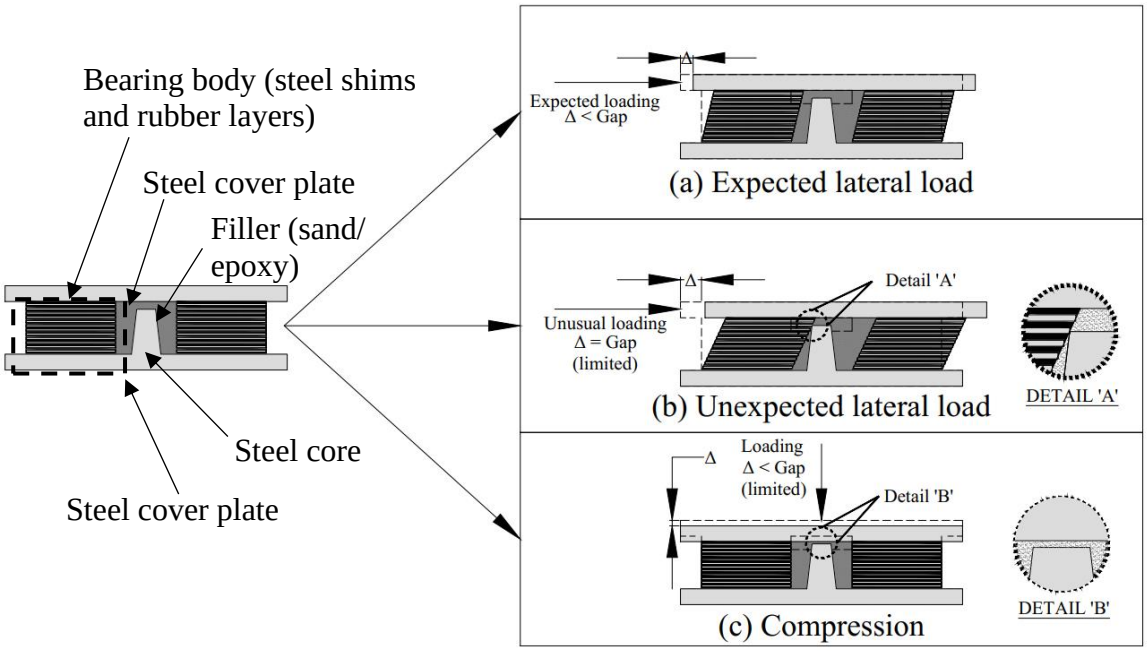

Fig. 1 Behaviour of core-and-filler system under various loading conditions

3.0 Development of Design Process for Proposed Elastomeric Bearing

In this research work, the required dimension of elastomeric bearing for considered design load is determined through a series of design steps that comply with the code of practice adopted in European industry, namely EN 1337-3. Structural bearings Part 3: elastomeric bearings [57]. During design stage, the filler properties are excluded. The dimensions of bearing components are determined solely based on the properties of rubber and steel, and design loading condition. Therefore, in this research, a special design process has been developed for the elastomeric bearing body that is compatible to core and filler system in accordance with EN1337-3: 2005. The developed design process is demonstrated step by step in follow and illustrated in Fig. 3:

1. Set the design axial load, F_v and total design displacement, *TDD*. The design axial load usually considers dead load and live load transferred from superstructure to the interested location where bearing sits. *TDD* on the other hand, can be determined from

either relevant code of practice or other considerations. In this study, the design axial load is 180kN, while the maximum displacement is set as 30mm.

2. Determine the shear modulus of rubber, *G* from Table 1, EN1337-3: 2005. It is recommended to be 0.9MPa based on the code of practice.

3. Identify the maximum bearing diameter, ϕ_b based on superstructure geometry and site constraints. This dimension should take the constructability into account. In this study, the overall diameter of bearing is taken as 275mm.

4. From *TDD* and ϕ_b determined in step 1 and 3 respectively, calculate the width of peripheral elastomeric bearing body, W_r by using Eq.(1). The bottom diameter of core, $\phi_{c,bot}$ can be set as any value that is less than two times *TDD*. It was taken as 0.5*TDD* in the present study to allow sufficient room for filler.
   Non-prismatic profile was proposed for steel core. The diameter of core reduced from 15mm at the bottom to 10mm at the top, where the core stem body sloped at a rise to run ratio of 14:1.

$$W_r = \frac{\phi_b - 2TDD - \phi_{c,bot}}{2} = \frac{275 - 2 \times 30 - 15}{2} = 100mm \quad (1)$$

5. Determine the plan area of at rest bearing, *A* and reduced effective area of bearing, A_r when it is displaced with the magnitude of *TDD* using Eqs.(3) and (4). The diameter of void, $\phi_{void} = 2TDD + \phi_{c,bot}$. Eq. (4) is derived from cl.5.3.3.2, EN1337-3: 2005 considering the bearing is displaced in only one direction.

$$\phi_{void} = 2TDD + \phi_{c,bot} = 2 \times 30 + 15 = 75mm \quad (2)$$

$$A = \pi \times \frac{(\phi_{void} + 2W_r)^2 - (\phi_{void})^2}{4} = \pi \times \frac{(75 + 2 \times 100)^2 - (75)^2}{4} = 54977.87mm^2 \quad (3)$$

$$A_r = A\left(1 - \frac{TDD}{\phi_{void} + 2W_r}\right) = 54977.87 \times \left(1 - \frac{30}{75 + 2 \times 100}\right) = 48980.28mm^2 \quad (4)$$

6. Set the number and thickness of rubber layers (n_r, $t_{r,i}$ and $t_{r,o}$), steel shims, (n_s and t_s) and cover plates (T_{top} and T_{bot}). The layer geometry should consider the space constraint due to structural design in terms of the gap allowable between the soffit of superstructure and top of substructure. The value of t_s should not be less than 2mm, in accordance with cl.4.3.3.1, EN1337-2: 2005.
   Calculate the total thickness of rubber, T_r. In any case, the shear strain should not exceed the limit stated in code of practice, which is 1 in accordance with cl.5.3.3.3, EN1337-3: 2005.
   The thickness of cover plates (T_{top} and T_{bot}) should be calculated alongside with the connection design as per relevant code of practice, as this dimension may affect the connection strength, such as bearing resistance for bolt group.
   In the present study, the thickness of steel shims and inner rubber layers is 3mm. 2 nos. outer rubber layer of 4mm thickness are provided, in addition to 9 nos. inner rubber layer. 10 nos. of steel shims are placed alternately with these rubber layers.

7. Determine the allowable pressure, P_{all} using Eq.(8), as per cl.5.3.3.6, EN1337-3: 2005. The shape factor for thickest elastomer layer, *S'* should only refer to the dimension of the thickest layer, as per cl.5.3.3.1, EN1337-3: 2005. Then, determine the pressure

exerted on elastomeric bearing due to compression, P_v using Eq.(9). The value of A and F_v are from step 5 and 1 respectively.

$$P = \pi \times [(\phi_{void} + 2W_r) + (\phi_{void})] = \pi \times [(75 + 2 \times 100) + (75)] = 1099.56mm \tag{5}$$

$$S' = \begin{cases} \dfrac{A}{P \times t_{eff}}, t_{eff} < 3 \\ \dfrac{A}{P \times 1.4t_{eff}}, t_{eff} \geq 3 \end{cases} = \frac{54977.87}{1099.56 \times 1.4 \times 4} = 8.93 \tag{6}$$

$$S = \frac{A}{P \times T_r} = \frac{54977.87}{1099.56 \times 35} = 1.43 \tag{7}$$

$$P_{all} = \frac{2(2W_r + \phi_{void})GS'}{3\sum_{k=1}^{n_r} t_{r,k}} = \frac{2(2 \times 100 + 75) \times 0.9 \times 8.93}{3 \times 35} = 42.1MPa \tag{8}$$

$$P_v = \frac{F_v}{A} = \frac{180 \times 10^3}{54977.87} = 3.28MPa \tag{9}$$

8. If the value of P_v is greater than P_{all}, go back to step 6 and reduce the thickness of rubber layers i.e. $t_{r,i}$ and $t_{r,o}$ to achieve smaller elastomer thickness. Otherwise, proceed to step 9.
   In this study, this criterion is fulfilled.

9. Determine the height of steel core, H_{core} that allows the bearing to settle under compression without allowing the contact between core and cover plate.
   In accordance with cl.5.3.3.7, EN1337-3: 2005, the vertical deflection of bearing under design load can be first calculated, and H_{core} should equals to the difference between T_r and the calculated deflection.
   However, it has been stated in the referred standard that 25% of variation may occur, and this needs to be taken into consideration. By allowing extra 5mm of vertical deflection as safety margin, Eq.(10) is produced and used to estimate the maximum vertical deflection attained.
   In this study, 30mm allowable vertical deflection is adopted and therefore, the height of core is 35mm, as calculated in Eq.(11).

$$D_{lim} \geq 1.25\left(\frac{F_v \sum_{k=1}^{n_r} t_{r,k}}{5AGS^2} + \frac{F_v \sum_{k=1}^{n_r} t_{r,k}}{AE_b}\right) + 5mm$$

$$D_{lim} \geq 1.25\left(\frac{180 \times 10^3 \times 35}{5 \times 54977.87 \times 0.9 \times 1.43^2} + \frac{180 \times 10^3 \times 35}{54977.87 \times 2000}\right) + 5mm$$

$$D_{lim} = 30mm \geq 20.6mm \tag{10}$$

$$H_{core} = (T_r + n_s t_s) - D_{lim} = (35 + 10 \times 3) - 30 = 35mm \tag{11}$$

10. Determine the plan dimension of cover plates (L_{top}, W_{top}, L_{bot} and W_{bot}) based on the design constraints identified in step 3. These dimensions are taken as 325mm.

Refer to Fig. 2 for the definition of key bearing dimensions. The output of the presented design workflow shown in Fig. 3 is the dimension of elastomeric bearing that is ready to implement core-and-filler system.

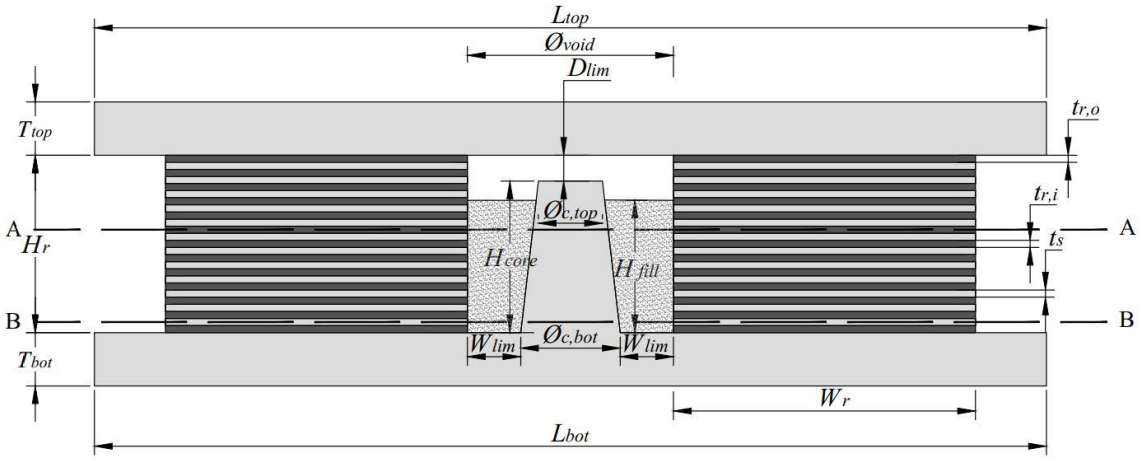

Fig. 2 Bearing dimensions

4.0 Behaviour of Proposed Rubber Elastomer Bearing with Granular or Polymer Filler

As showed in Fig. 4, three types of proposed bearings were considered to study the behaviour of elastomer bearing with both granular and epoxy filling mechanism.

The bearing with granular filler with partially filled condition named as SCRB1 (Sand-Core Rubber Bearing 1) to compare its performance with the same bearing with fully filled condition which named as SCRB2 (Sand-Core Rubber Bearing 2) in order to assess effect of partially and fully filler system on overall performance of bearing.

For polymer filler, only fully filled condition is used and named as ECRB (Epoxy-Core Rubber Bearing).

Therefore, in order to conduct comparable study, a bearing with details as showed in Fig. 5 is considered. The overall dimension of the bearing is 275mm diameter by 65mm height. 75mm diameter central void is provided, along with 100mm width ring-shaped elastomeric bearing body. The height of filler as 35mm and the top of sand filler flushed with the top of steel core. The volume of filler for fully filled and partially filled conditions were 282,694mm^3 and 150,158mm^3 respectively.

The performance of proposed elastomeric bearings is compared against conventional laminated rubber bearing (LRB) and lead-core rubber bearing (LCRB) with the same diameter and height. For LRB, void is not presented at the centre of bearing body, while for LCRB the void is plugged with 75mm diameter lead core.

Study about behaviour of above-mentioned bearing has been made through numerical simulation via the finite element method which the details are demonstrated in the next sections.

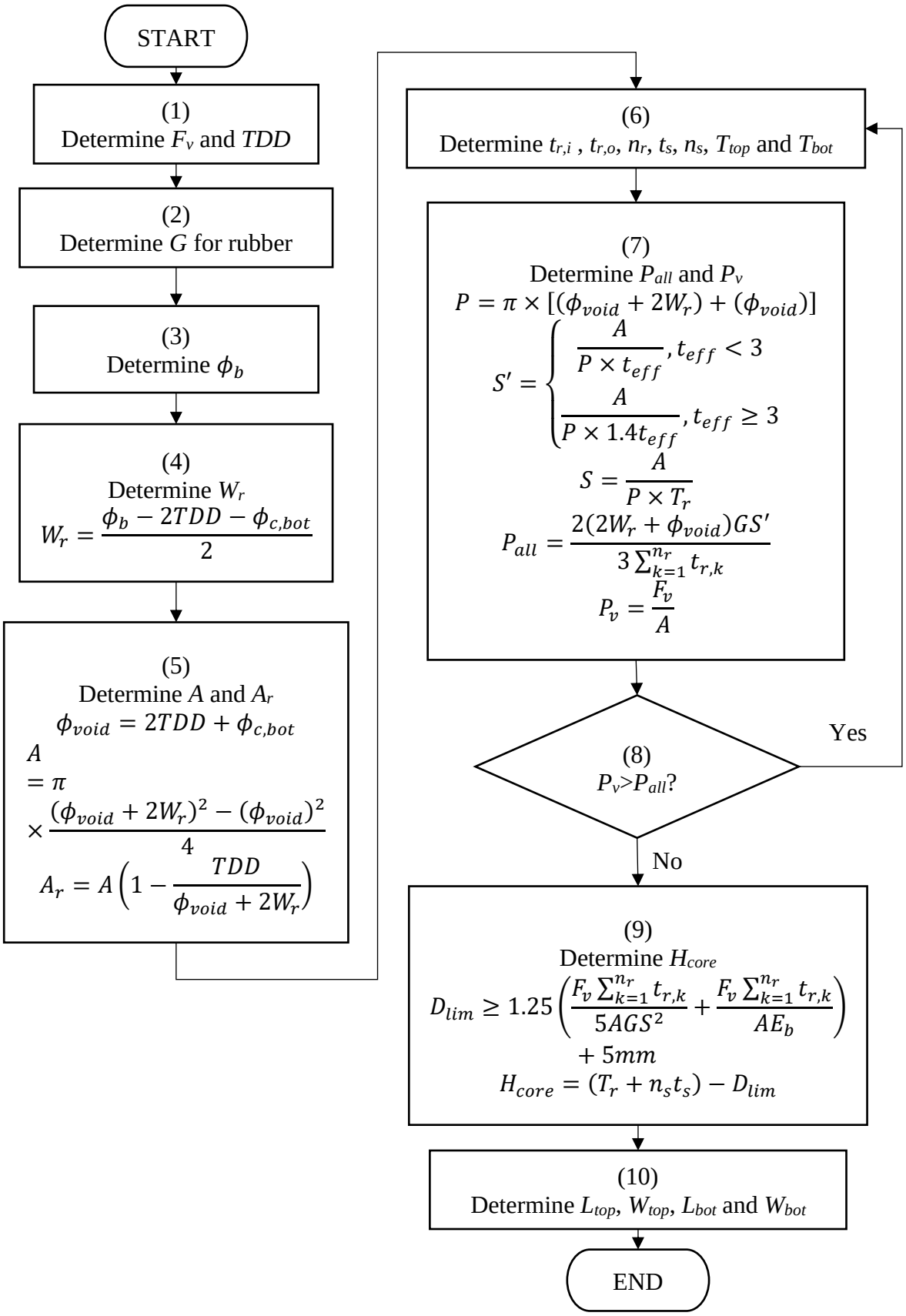

Fig. 3 Design workflow developed for proposed elastomeric bearing

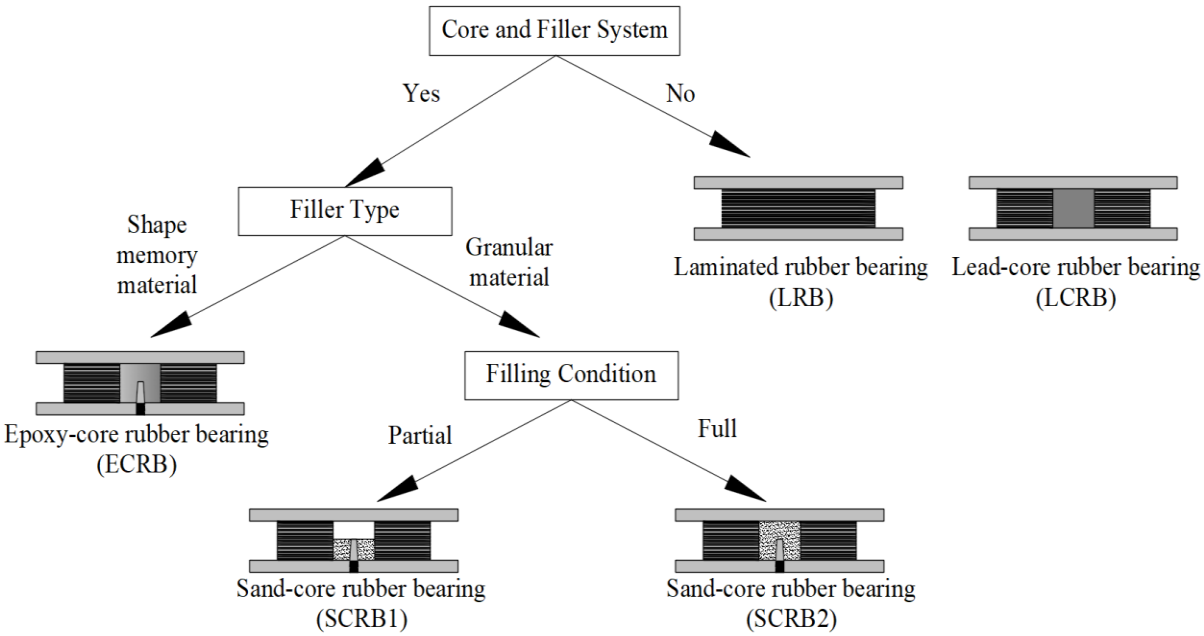

Fig. 4 Bearing models simulated in the present study

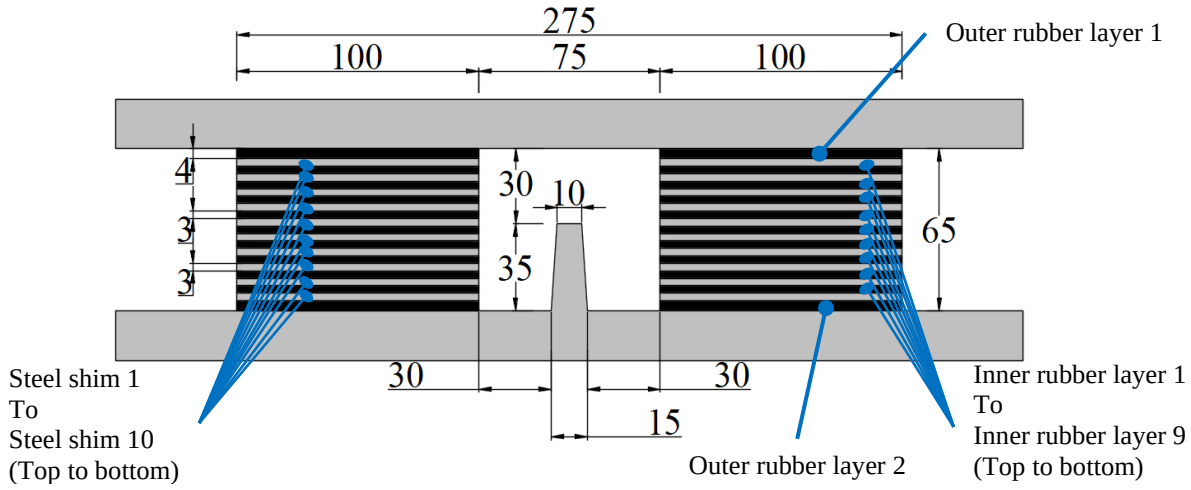

Fig. 5 Dimension of components in elastomeric bearing equipped with proposed core-and-filler system

5.0 Finite Element Modelling of Considered Bearings

As mentioned in the previous section, as showed in Fig. 4, all following proposed bearings with core-filler mechanism and also conventional bearings as benchmark for comparison the results are considered to study using finite element method:

(i) SCRB1: Sand-Core Rubber Bearing with partial filling condition
(ii) SCRB2: Sand-Core Rubber Bearing with fully filling condition
(iii) ECRB: Epoxy-Core Rubber Bearing
(iv) LRB: Laminated Rubber Bearing
(v) LCRB: Lead-Core Rubber Bearing

The ABAQUS software was used to develop finite element models of mentioned elastomeric bearings. Simulations were conducted on the developed models which the geometry details have been demonstrated in Fig. 5, and then their analysis outputs were extracted for data processing and interpretation.

5.2 Material properties

This section presents the definition of the mechanical properties for all material used in the developed elastomeric bearing model in simulation via finite element method.

5.2.1 Rubber

During the design stage, the shear modulus of rubber was taken as 0.9MPa, where 0.15MPa of tolerance was allowed [57].

Rubber exhibits linear stress-strain relationship under small strain. On the other hand, the relationship becomes non-linear when it is subjected to large strain. This can be observed from uniaxial test result for rubber, such as one conducted by Treloar [34]. Nonetheless, despite under behaves in non-linear fashion, the material remains elastic and ready to restore to its original shape upon unloading.

This behaviour of rubber is governed by hyperelastic model, while considering the material itself to be isotropic. Among the various hyperelastic model offered in ABAQUS [58], 3rd order Ogden model was implemented for its accuracy [44]. Eq.(12) presents the strain-energy function *W* defined in 3rd order Ogden model [58]:

$$W = \sum_{i=1}^{3} \frac{2\mu_i}{\alpha_i^2}\left[\lambda_1^{\alpha_i} + \lambda_2^{\alpha_i} + \lambda_3^{\alpha_i} - 3\right] \tag{12}$$

In Eq.(12), principal stretches of rubber are represented by λ_1, λ_2 and λ_3. Material constants μ_i and α_i are the parameters that define the behaviour of rubber under loading. The material constants adopted in this study are shown in Table 1 [59].

Table 1 3rd order Ogden hyperelastic model parameters defined for rubber

	μ	α
1	0.3326	2.4466
2	0.3326	2.4466
3	0.3326	2.4466

The shear modulus, G_0 of the is 0.9978MPa, which is within the allowable tolerance of 0.15MPa from mean value of 0.9MPa. Refer to Eq. (13) for the determination of G_0 [58]. As remarked by Altalabani et al. (2021), Mullins effect was neglected to simplify the analysis [60].

$$G_0 = \sum_{i=1}^{N} \mu_i = 0.9978MPa \tag{13}$$

The initial bulk modulus K_0 was taken as 2000MPa [57]. Poisson's ratio, ν is as calculated in Eq. (14), knowing the value of G_0 is 0.9978MPa [58]:

$$\nu = \frac{3\,K_0/G_0 - 2}{6\,K_0/G_0 + 2} = \frac{3(2000/0.9978) - 2}{6(2000/0.9978) + 2} = 0.4998 \tag{14}$$

High v is produced from high K_0/G_0 ratio, and this indicates the compressibility of rubber is negligible comparing to its flexibility under shear. Therefore, rubber is treated as incompressible material.
Another important characteristic of rubber is energy dissipation through damping. In numerical analysis, such behaviour is taken into account by defining Bergstrom-Boyce hysteresis parameters. In present study, adopted hysteresis parameters are presented in Table 2.

Table 2 Bergstrom-Boyce hysteresis model parameters for rubber

Stress scaling factor S	Creep parameter $\hat{C}_1$	Effective stress exponent m	Creep strain exponent C_2
50	4×10^{-10}	8	0

5.2.2 Steel
The elastic behaviour of steel is defined by using modulus of elasticity E of 210GPa and Poisson's ratio v of 0.3 [61]. As for plasticity, steel is set to yield at 235MPa, while its ultimate strength is set as 360MPa with corresponding strain of 25% [57][61] (Refer to Table 3).

5.2.3 Sand
In the present study, finite element method is favoured for lower computational cost compared to discrete element method [50]. The sand mass properties are governed by elastic model, with modulus of elasticity E of 85MPa and Poisson's ratio v of 0.3 [62][63] (Refer to Table 3).

5.2.4 Epoxy
The behaviour of epoxy is described using elastoplastic model. Its modulus of elasticity E was taken as 1038MPa, while Poisson's ratio v of 0.35 was adopted [64]. For plasticity, the yield stress σ_y of epoxy was set as 15.8MPa with the corresponding yield strain ε_y of 1.07%. Ultimate stress σ_{max} of 26.5MPa was set, and the corresponding elongation at break ε_{max} was defined as 2.9% [65] (Refer to Table 3).

5.2.5 Lead
The elastic properties of lead were defined using modulus of elasticity E of 10GPa and Poisson's ratio v of 0.43 [60]. The yield strength of lead was taken as 10MPa [6].
Table 3 summarizes of properties defined for continuum materials in the simulation.

5.3 Model Meshing
All bearing components are meshed using hex shape element. Elastomer component i.e. rubber layer was meshed using reduced integration linear hexahedral solid element with eight-node and three degree of freedom under hourglass control and hybrid with constant pressure (C3D8RH). Linear triangular prism with six-node and three degree of freedom (C3D6) element was adopted for sand mass. Reduced integration linear hexahedral solid element with eight-node and three degree of freedom under hourglass control (C3D8R) element was used to model the remaining components.

5.4 Interactions
The soffit of bottom cover plate is expected to be fixed throughout the analysis. Therefore, encastre boundary condition was defined. As for the top plate, only translational movements along x and z directions, due to shear and axial forces respectively were allowed. The top plate was restrained against rotation. This definition simulated the condition where the superstructure possesses very high rotational stiffness [66].

Table 3 Mechanical properties of steel, sand, epoxy and lead

Material	Mechanical Properties
Steel	E=210GPa [61]
	ν=0.3 [61]
	σ_y=235MPa [57]
	ε_y=0.11% [61]
	σ_u=360MPa [61]
	ε_u=25% [61]
Sand	E=85MPa [62][63]
	ν=0.3 [62][63]
Epoxy	E=1038MPa [64]
	ν=0.35 [64]
	σ_y=15.8MPa [65]
	ε_y=1.07% [65]
	σ_u=26.5MPa [65]
	ε_u=2.9% [65]
Lead	E=18GPa [60]
	ν=0.43 [60]
	σ_y=10MPa [6]

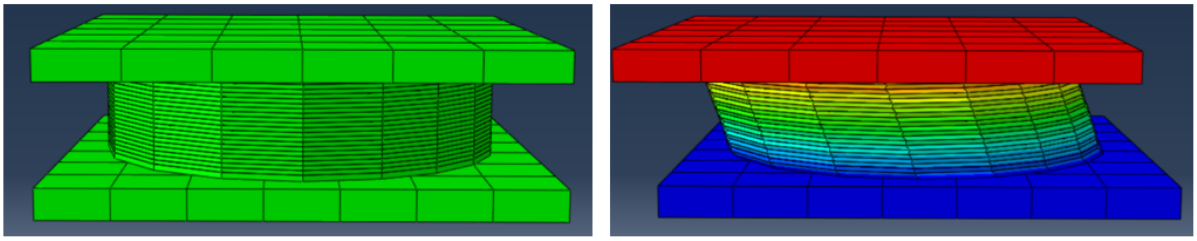

(a) Unloaded condition (b) Deformation during cyclic shear test

Fig. 6 Proposed elastomeric bearing during finite element simulation

Tie constraint was defined for contact interfaces among all the bearing components, namely cover plates, rubber layers, steel shims, steel core, lead core and filler.

For steel-rubber contact interface, this definition simulates the adhesion between those components which formed via vulcanization involving heat and pressure [67]. Same behaviour was set for contact between cover plates and outer rubber layers. Although modelled as separate entities, both steel core and bottom cover plate are tied together, indicating the condition where the threaded connection between the core and bottom plate is anticipated to be intact during the bearing operation. For epoxy, adhesion is developed after the filling and curing process. For sand material, tangential contact between sand mass surface and bearing components can be defined as rough contact, where the slippage of contacting interfaces should not occur [68]. In addition, the sand mass surface should remain contact with the bearing components in normal direction, neither penetration nor separation will occur. Use of tie constraint for contact between lead core and bearing components has been proven adequate in literature [60].

5.5 Characteristics of elastomeric bearing

In this study, the behaviour of elastomeric bearing is described using equivalent damping ratio h_{eq}, effective stiffness k_{eff}, dissipated energy ED and yield force Q. To determine these parameters, the final cycle of lateral force-displacement curve from the simulation of cyclic

shear test is referred. The calculation methods for these characteristics are presented in Eqs. (15), (16) and (17) [60][11]:

$$h_{eq} = \frac{2ED}{\pi k_{eff}\left(d_p - d_n\right)^2} \tag{15}$$

$$k_{eff} = \frac{F_p - F_n}{d_p - d_n} \tag{16}$$

$$Q = \frac{1}{2}\left(Q_p - Q_n\right) \tag{17}$$

In these equations (Eqs. (15), (16) and (17)), the applied strokes in positive and negative directions are represented by d_p and d_n. Forces required to cause the displacement of d_p and d_n are F_p and F_n respectively. Q_p and Q_n are the yield force at positive and negative sides respectively. *ED* is defined as energy dissipated throughout one cycle, and it can be measured directly based on the area under the hysteresis loop from the curve shown in Fig. 7.

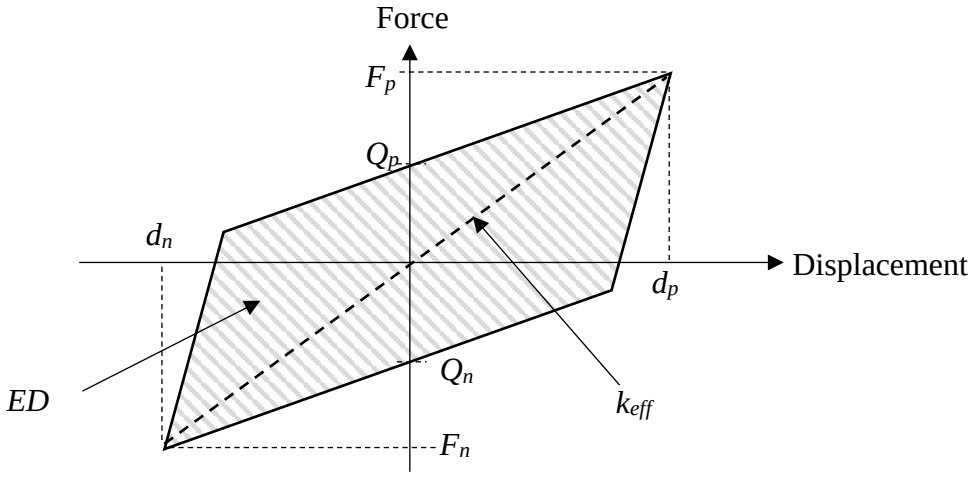

Fig. 7 Parameters and characteristics of elastomeric bearing in lateral force-displacement curve

5.6 Simulation of design condition

Design stroke was exerted at the midpoint of top plate. Finite element nodes on the top surface of the cover plate are connected to the loading point by the mean of multi-point constraint [58]. Design axial load of 180kN was exerted on this loading point as a concentrated load.

On top of that, 30mm design lateral displacement was applied to the loading point. It was defined as three sinusoidal cycles of horizontal displacement with the frequency of 0.0556Hz, equivalent to the circular frequency of 0.349rad/s. Corresponding to the frequency, the time taken to complete one cycle is 18s. Three cycles of lateral stroke was simulated, where the force-displacement relation for the final cycle was used to derive the characteristics of elastomeric bearing. Fig. 8 illustrates the displacement applied during the finite element analysis.

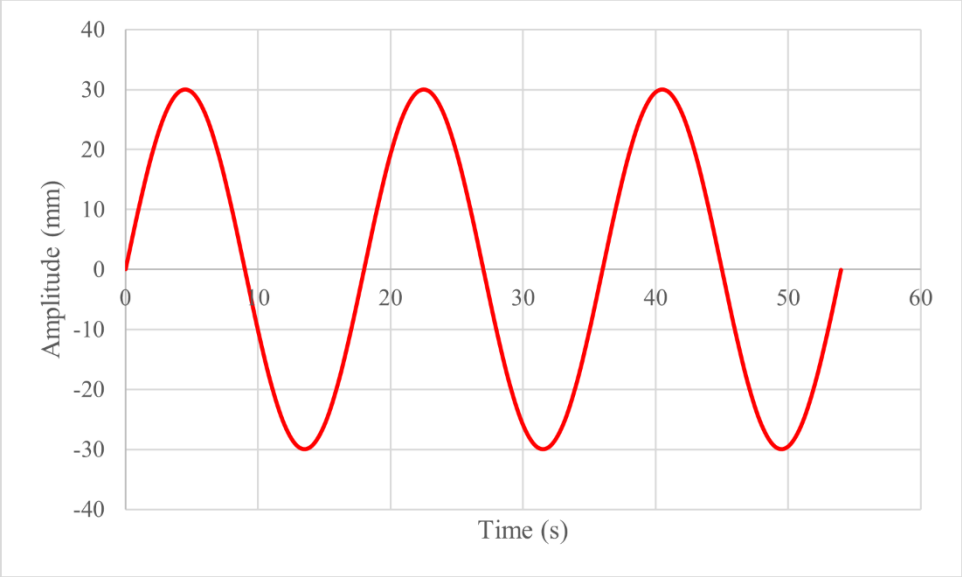

Fig. 8 Applied sinusoidal displacement during the simulation of design condition

Through simulation process, at the first step, the design axial load was applied to the bearing. Then, cyclic lateral displacement was exerted while maintaining the axial load. This simulates the condition where axial force and lateral stroke are simultaneously loaded on the bearing. The proposed core and filler system with both sand and epoxy are first simulated and compared against the lead core under the design loading to inspect the behaviour of core system. The strength of lead core is inferior when compared to that of proposed core system. Steel core utilizing epoxy filler possesses the highest strength and damping among all the systems. Fig. 9 compares the hysteresis behaviour of all three core systems.

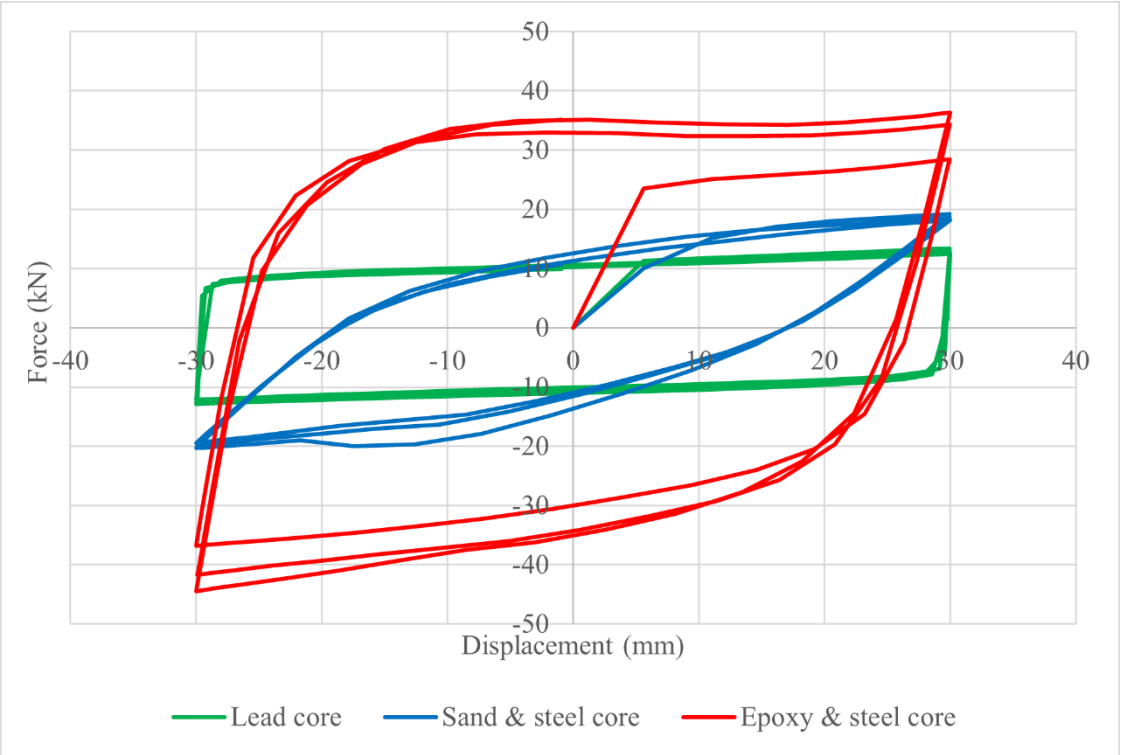

Fig. 9 Simulation result for proposed core systems and lead core

Then, the bearings are simulated their stress distribution are determined. Stress developed in steel shims and rubber layers of LRB is the lowest among all the simulated elastomeric bearings. The stress developed in rubber layer remains consistent for all types of bearings, with the increment of up to 17.8% as observed in SCRB2 when compared to LRB.
For LCRB, SCRB2 and ECRB, the stress in steel shims first decreases top down until the top level of steel core (from steel shim 1 to steel shim 6), and then it increases until the bottom cover plate level (from steel shim 6 to steel shim 10). Steel shim 1 and 10 experiences highest stress, as they are located near to the high stress stiff region, where the core system contacts with both top and bottom cover plates. However, this is not the case for partially filled SCRB1. The stress developed in steel shims of LRB shows large difference when compared to the others. Among the bearings utilizing core, steel shims in LCRB experience the highest stress with the maximum of 248.3MPa. Three steel shims (steel shim 1, 9 and 10) are found yielded throughout the simulation. For bearing with proposed system, the stress in steel shims is the highest in SCRB2 (241.4MPa), followed by ECRB (239.6MPa) and SCRB1 (236.5MPa). For both SCRB2 and ECRB, the topmost steel shim 1 is found yielded. Steel shims 5, 6 and 10 are yielded for SCRB1. Steel shim 5 is partially covered by the filler. When stroked, the steel shim section experiences high shear and this causes the development of high stress.
For elastomeric bearing equipped with the proposed system, the steel core experiences high stress at the root level and yielding is expected. For LCRB, lead core is found yielded as well. Among the simulated bearing, the stress developed in top cover plate is the highest for LCRB (194MPa). Given lower yield strength, lead core experiences earlier yielding when compared to the steel core. As a result, force associated with the stroking is mainly resisted by the top cover plate, and this leads to high stress in the steel plate. For elastomeric bearing with proposed core and filler system, the stress in bottom cover plate is greater than that developed in top cover plate. This connection with steel core enables the transfer of stress to bottom cover plate and thus making the developed stress higher when compared to top cover plate.
Table 4 shows the maximum stress developed in all components for each type of bearing. Fig. 10 shows the stress contour obtained from finite element analysis.

6.0 Parametric study

Several parameters were set as manipulating variable to investigate their effect on the performance of elastomeric bearing. In present study, the geometry of bearing components was not studied, as the purpose of this parametric study was to identify the change in the behaviour of bearing due to the uncertainties that may happen during fabrication and service. Instead, the study focusing on two main aspects, namely material properties and loading conditions.

6.1 Material properties correlation

Among all materials used, the mechanical properties of sand are rather inconsistent as they are dependent on their packing state. For instance, the modulus of elasticity for dense sand is greater than that for loose sand. Even so, the mechanical properties of sand with the same packing state category may vary hugely, since they are not only affected by the arrangement of sand grains, but also loading history and density [69].
Parametric study on the effect of sand properties on the characteristics of SCRB1 and SCRB2 was conducted due to the potentially large variability in terms of sand properties. In relation to that, 8 cases were defined, as listed in Table 5. The range of sand parameters was based on the extreme values recommended by Bowles for loose and dense sand [69].

Table 4 Maximum stress developed in the components of simulated bearings

	Maximum stress (MPa)				
Component	LRB	LCRB	SCRB1	SCRB2	ECRB
Top cover plate	2.7	194	3.3	36.1	35.7
Bottom cover plate	13.9	66	42.4	74.8	74.9
Core (lead / steel)	-	10	360	360	360
Filler	-	-	22.8	41.9	23.7
Outer rubber layer 1 (top)	11.8	11.9	13.3	13.9	13.1
Steel shim 1	22.9	248.3	50.9	241.4	239.6
Inner rubber layer 1	11.8	12.3	13.3	12.6	11.8
Steel shim 2	20.8	225.1	65.8	206.3	183.6
Inner rubber layer 2	11.8	11.4	13.3	12.1	11.3
Steel shim 3	19.5	189.6	78.1	175.9	160.6
Inner rubber layer 3	11.8	12.1	13.3	12.1	11.2
Steel shim 4	19.5	144.8	96.3	150.5	136.9
Inner rubber layer 4	11.8	12	13.3	12.1	11.2
Steel shim 5	18.9	160.9	236.5	155.9	153.4
Inner rubber layer 5	11.8	11.3	10.1	12.5	11.9
Steel shim 6	18.9	151.4	235.5	137	131.6
Inner rubber layer 6	11.8	12	10.2	12.5	11.8
Steel shim 7	19.7	202.8	232.6	157	171.5
Inner rubber layer 7	11.8	12.1	10.2	12.3	11.3
Steel shim 8	20.1	224.2	229.1	185.3	181.1
Inner rubber layer 8	11.8	11.3	10.1	12.3	11.4
Steel shim 9	20.8	235.1	201.1	234.1	214.5
Inner rubber layer 9	11.8	12.1	10	11.8	11.3
Steel shim 10	25.5	235.7	235.2	222.9	231.9
Outer rubber layer 2 (bottom)	11.8	11.5	11.1	13.8	13.1

Table 5 Material properties of SCRB1 and SCRB2 for material properties study

Simulation case	Rubber G (MPa)	Sand E (MPa)	Sand v
M1	0.9978	10	0.2
M2	0.9978	10	0.3
M3	0.9978	25	0.2
M4	0.9978	25	0.3
M5	0.9978	50	0.2
M6	0.9978	50	0.3
M7	0.9978	81	0.2
M8	0.9978	81	0.3

The variability of sand properties influences on the bearing characteristics of SCRB1 and SCRB2.

The equivalent damping ratio of bearing varies from 25.16% to 25.94% for SCRB1, and 19.52% to 23.56% for SCRB2. When the sand mass in SCRB1 changes from its densest state to the loosest state, the values of h_{eq} and Q change by +3.1% and -1.5% respectively. For SCRB2, the changes in h_{eq} and Q under the same situation are +20.7% and -0.4% respectively.

In terms of stiffness, the range of variation lies between 12.79kN/mm to 13.32kN/mm for SCRB1 and 14.59kN/mm to 17.26kN/mm for SCRB2.

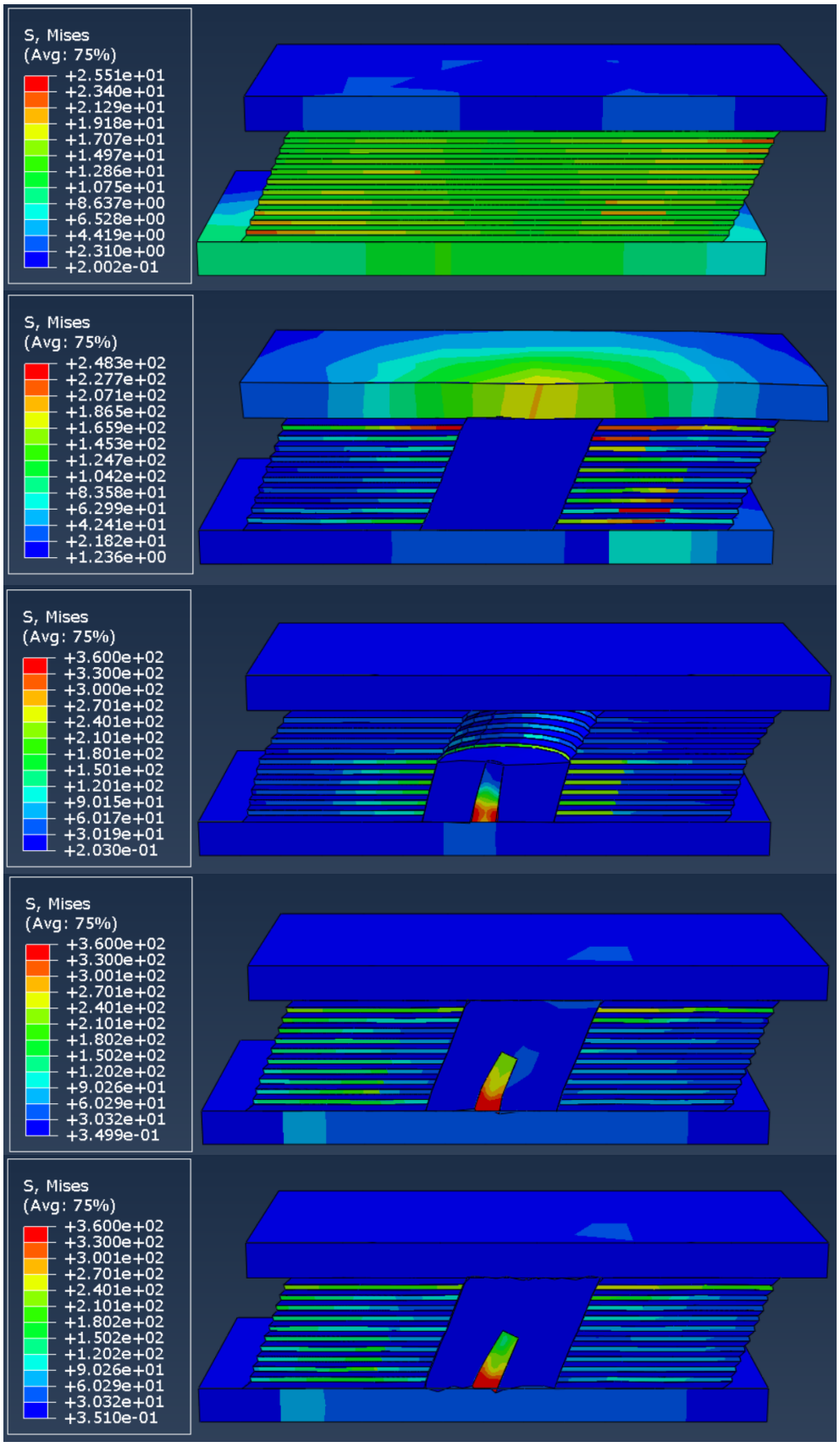

Fig. 10 Maximum stress in simulated elastomeric bearings

Table 6 Bearing characteristics obtained from finite element analysis for SCRB1 and SCRB2 under simulation case M1 to M8 and benchmark case

	SCRB1				SCRB2			
Simulation case	*ED* (kNmm)	h_{eq} *(%)*	k_{eff} (kN/mm)	*Q* (kN)	*ED* (kNmm)	h_{eq} *(%)*	k_{eff} (kN/mm)	*Q* (kN)
Benchmark	18948	25.16	13.32	390.9	19055	19.52	17.26	379.8
M1	18758	25.94	12.79	385.2	19417	23.53	14.60	378.2
M2	18759	25.94	12.79	385.2	19418	23.56	14.59	378.2
M3	18795	25.72	12.92	386.6	19343	22.30	15.35	378.6
M4	18797	25.71	12.93	386.7	19347	22.36	15.31	378.7
M5	18858	25.44	13.11	388.7	18637	20.40	16.17	379
M6	18861	25.44	13.11	388.7	18835	20.72	16.09	379.1
M7	18935	25.18	13.3	390.6	18789	19.34	17.19	379.6
M8	18938	25.18	13.3	390.7	18896	19.60	17.06	379.7

This shows the reduction of 4% and 15.5% are achievable for k_{eff} of SCRB1 and SCRB2 respectively, from the highest possible stiffness. For *ED*, the value ranges from 18758kNmm to 18948kNmm for SCRB1, and from 19055kNmm to 19418kNmm for SCRB2. The reduction from peak value is 1.0% and 1.9% for SCRB1 and SCRB2 respectively. Refer to Table 6 for the tabulation of simulation results.

6.2 Loading conditions correlation

The influence of loading conditions was studied in several aspects. The first aspect was loading frequency, where study was done by establishing 3 different frequencies. In the simulation, the applied lateral displacement was set as 30mm. The displacement pattern was maintained as sinusoidal to enable comparison with the benchmark performance.

Correlation between the displacement pattern and bearings characteristics was also investigated by applying triangular displacement. The lateral displacement and frequency were set as 30mm and 0.0556Hz respectively. Unlike sinusoidal displacement, the loading rate for triangular displacement was consistent at 6.7mm/s throughout the simulated period.

Other than constant amplitude, elastomeric bearings behaviour under increasing amplitude was studied as well to obtain insight on the correlation between loading history and isolation performance of elastomeric bearings when comparing with the result obtained from case L4. Under the frequency of 0.0556Hz, the amplitude of lateral displacement increases by 5mm after every cycle. The loading started from 5mm and ended at *TDD*, 30mm. In relation to this pattern, the loading rate increases by 1.117mm/s in every subsequent cycle, began with 1.117mm/s and ended at 6.7mm/s. During evaluation, the final cycle with 30mm amplitude was referred to derive the characteristics of elastomeric bearings. Fig. 11 and Fig. 12 shows the adopted displacement for the studies.

The hysteresis behaviour of elastomeric bearings was also explored under different lateral displacement. The analysis cases were divided into two categories. The first category was the situation where the bearings was stroke with displacement smaller than *TDD*. For this category, five cases were studied. The second category was the situation where the applied lateral displacement exceeded *TDD*. Under this category, three cases were simulated, covering 100%, 150% and 200% shear strain, based on the total elastomer layers thickness of 35mm. Other controlling parameters such as frequency and displacement pattern were maintained as it was for design condition.

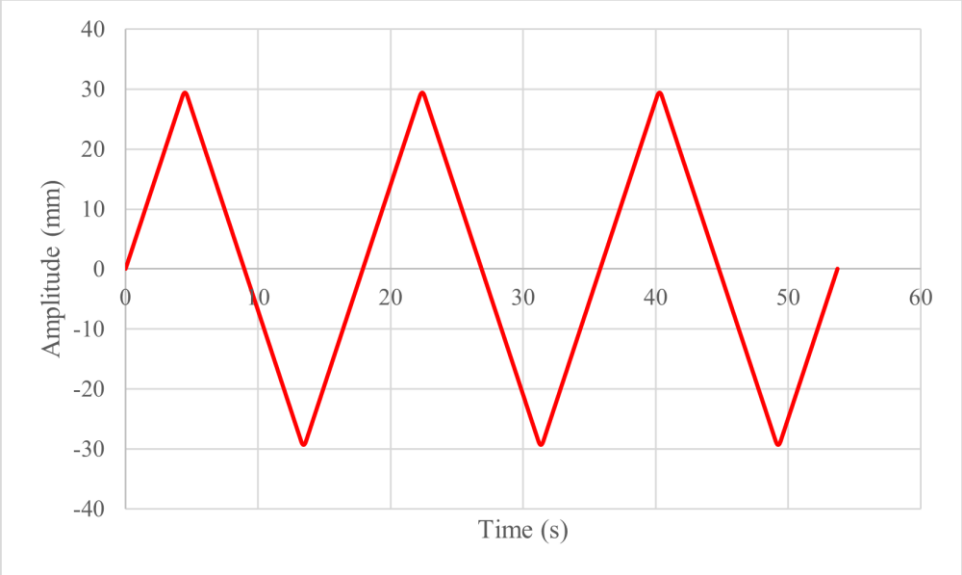

Fig. 11 Triangular displacement applied on the elastomeric bearings

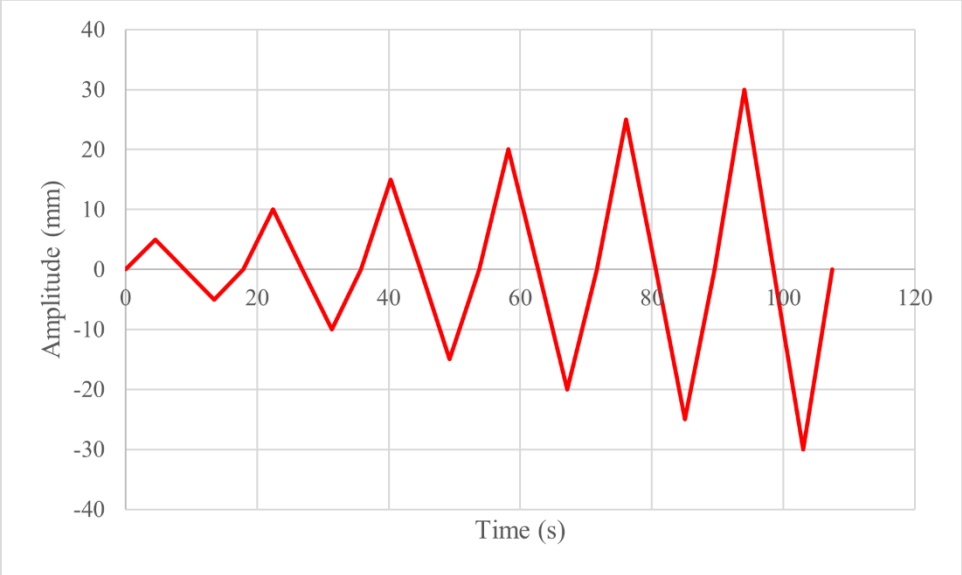

Fig. 12 Triangular displacement with increasing amplitude applied on the elastomeric bearings

Table 7 summarizes the simulated cases for the parametric investigation involving loading conditions. Generally, when subjected to cases under different frequencies, *ED*, h_{eq}, k_{eff} and *Q* of bearing increases with frequency, except for LRB where the equivalent damping ratio decreases under these loading conditions. The results are presented in Table 8.

The bearing characteristics obtained from simulation case L4 was compared to that from benchmark to gain insight on the effect of displacement pattern. The deviation between two sets of data were tabulated together with the output in Table 9. The hysteresis curve obtained are shown in Fig. 13. Qualitatively, the vertices of hysteresis curve subjected to triangular displacement was found sharper than that from sinusoidal displacement. Such behaviour shrinks the area inside the hysteresis curve and led to reduction in terms of *ED* and h_{eq}. On the other hand, k_{eff} increased when compared to benchmark. At the same time, *Q* decreased.

Table 7 Loading conditions used in parametric study

Simulation case	Displacement pattern	Amplitude (mm)	Frequency (Hz)
L1	Sinusoidal	30	0.0167
L2	Sinusoidal	30	0.0333
L3	Sinusoidal	30	0.05
L4	Triangular	30	0.0556
L5	Triangular	5 to 30	0.0556
L6	Sinusoidal	5	0.0556
L7	Sinusoidal	10	0.0556
L8	Sinusoidal	15	0.0556
L9	Sinusoidal	20	0.0556
L10	Sinusoidal	25	0.0556
L11	Sinusoidal	35	0.0556
L12	Sinusoidal	52.5	0.0556
L13	Sinusoidal	70	0.0556

Table 8 Characteristics of bearings under various loading frequencies

Bearing	Case	Frequency (Hz)	*ED* (kNmm)	h_{eq} *(%)*	k_{eff} (kN/mm)	*Q* (kN)
LRB	L1	0.0167	11087	17.66	11.10	359.0
	L2	0.0333	11823	17.48	11.96	390.6
	L3	0.05	12255	17.34	12.50	410.3
LCRB	L1	0.0167	18157	24.38	13.17	346.6
	L2	0.0333	19514	24.74	13.95	375.9
	L3	0.05	20338	24.92	14.43	394.2
SCRB1	L1	0.0167	16747	25.49	11.62	335.7
	L2	0.0333	17996	25.60	12.43	365.1
	L3	0.05	18754	25.63	12.94	383.3
SCRB2	L1	0.0167	16776	18.78	15.80	328.3
	L2	0.0333	18071	19.26	16.59	357.1
	L3	0.05	18856	19.51	17.09	375.0
ECRB	L1	0.0167	20335	23.81	15.10	400.2
	L2	0.0333	21602	24.04	15.89	428.8
	L3	0.05	22349	24.11	16.39	446.6

By comparing the results obtained from case L4 and L5, the force corresponding to maximum displacement was found greater for case L5 (refer to Fig. 14). Bearings with proposed mechanism exhibited lower h_{eq} (-4.4%, -7.2% and -1.2% for SCRB1, SCRB2 and ECRB respectively) and higher k_{eff} (+4.1%, +7.2% and +5.9% for SCRB1, SCRB2 and ECRB respectively) when subjected to triangular displacement with increasing amplitude. Given the same trend, the magnitude of change in h_{eq} and k_{eff} are the greatest for LCRB when compared to other bearings.

ED decreased insignificantly (0.4% for SCRB1 and SCRB2), although that was not the case for LRB and ECRB (+2.4% and +4.7%). The effect of loading history is found the greatest on LCRB, where the absolute change in bearing performances is considerably high when compared to other types of bearing, if not the highest. See Table 10 for the comparison of bearing characteristics under case L4 and L5.

Fig. 15 and Fig. 16 compare the hysteresis behaviour of elastomeric bearings against benchmark LRB and LCRB. From this comparison, the relative performances of proposed

bearings are consistent with that under benchmark loading condition, regardless of the types of displacement pattern and loading history. For instance, the lateral stiffness of SCRB2 remains higher than LCRB whether it is subjected to sinusoidal or triangular displacement.

Table 9 Characteristics of elastomeric bearings under simulation case L4 and their difference from benchmark design condition

Bearing	LRB		LCRB		SCRB1		SCRB2		ECRB	
	L4	Δ (%)	L4	Δ (%)	L4	Δ (%)	L4	Δ (%)	L4	Δ (%)
ED (kNmm)	11119	+0.1	18824	-8.4	17416	-8.1	17535	-7.9	20761	-7.4
h_{eq} *(%)*	13.47	-11.5	22.40	-8.9	20.73	-17.6	16.22	-17.0	20.03	-15.3
k_{eff} (kN/mm)	14.6	+13	14.86	+0.5	14.86	+11.6	19.12	+10.9	18.33	+9.4
Q (kN)	383.6	-8.3	360.6	-10.2	359.4	-8.1	350.7	-7.7	422.2	-7.0

Table 10 Characteristics of bearings under different loading history

Characteristics	Case	LRB	LCRB	SCRB1	SCRB2	ECRB
ED (kNmm)	L4	11119	18824	17416	17535	20761
	L5	11380	18779	17347	17463	21731
	Difference (%)	+2.4	-0.2	-0.4	-0.4	+4.7
h_{eq} *(%)*	L4	13.47	22.40	20.73	16.22	20.03
	L5	13.10	19.66	19.82	15.06	19.80
	Difference (%)	-2.7	-12.2	-4.4	-7.2	-1.2
k_{eff} (kN/mm)	L4	14.60	14.86	14.86	19.12	18.33
	L5	15.36	16.89	15.48	20.50	19.41
	Difference (%)	+5.2	+13.7	+4.1	+7.2	+5.9
Q (kN)	L4	383.6	360.6	359.4	350.7	422.2
	L5	378.1	347.9	352.9	346.8	419.1
	Difference (%)	-1.4	-3.5	-1.8	-1.1	-0.8

Constitutive curves of bearings were derived based on the maximum force corresponding to the maximum lateral displacement acquired from simulation case L6 to L13. The results are presented in Table 11, and Fig. 17 shows the constitutive curves developed for each bearing.
Fig. 18 demonstrates the hysteresis curves of bearings under excessive shear strain i.e. 100%, 150% and 200%.
Based on the observation, force required to push the top plate of bearing increased drastically when LCRB, SCRB2 and ECRB achieved around 150% shear strain i.e. from 700.7kN to 1173.4kN at 200% shear strain for LCRB (+67.5%), from 922.4kN to 1835.0kN at 200% shear strain for SCRB2 (+98.9%), and from 791kN to 1377.7kN at 200% shear strain for ECRB (+74.2%). On the other hand, such trend was not observed from the behaviour of LRB and SCRB1 with the comparatively low changes of +11.5% and +17.6% respectively.

7.0 Application of Proposed Bearing in a Building

The application of elastomeric bearings in a building as base isolator was simulated with ground motion record using finite element software, ETABS. The purpose of such simulation was to assess the structural response with proposed base isolator, where insights was obtained by comparing with fixed base condition as a benchmark.

Table 11 Force in bearings corresponds to the amplitude of lateral displacement under simulation case L6 to L13

Displacement	Force (kN)				
(mm)	LRB	LCRB	SCRB1	SCRB2	ECRB
-70	-493.7	-1151.9	-578.3	-1874.0	-1316.5
-52.5	-442.9	-685.4	-490.9	-981.3	-767.7
-35	-394.7	-468.3	-414.1	-593.0	-548.3
-30	-381.0	-434.4	-387.4	-511.0	-495.3
-25	-367.1	-406.0	-373.8	-470.3	-464.9
-20	-352.7	-380.8	-354.0	-425.0	-436.1
-15	-337.2	-356.6	-333.5	-382.4	-405.3
-10	-319.6	-334.2	-310.8	-340.5	-370.4
-5	-296.3	-271.1	-281.1	-294.5	-327.7
5	301.5	272.9	285.9	294.5	331.4
10	327.1	340.0	317.7	342.1	374.8
15	346.3	368.0	341.9	385.1	411.2
20	363.1	394.7	363.6	428.4	444.8
25	378.6	421.9	384.4	474.1	476.7
30	393.5	452.2	398.8	524.1	509.7
35	408.0	487.8	426.4	597.6	559.5
52.5	458.6	700.7	505.2	922.4	791.0
70	511.3	1173.4	594.0	1835.0	1377.7

7.1 Building data

The considered building structure is a five-storey office building based on an actual building located in Malaysia. The height of first storey is 4.267m, and subsequent four storeys are 3.353m height each. On top of roof floor, upper roofs of 4.8m height exist on top of lift motor room and staircases that provide access to roof floor. The total height of the building structure is 22.479m.

The lateral resistance of structure is mainly contributed by 230mm thick reinforced concrete shear wall that acts as lift core. Grid of columns are used to support the horizontal elements namely beams and slabs. The shape of perimeter column is rectangular, and that for interior column is circular. The concrete grade for beams and slabs is C25, while that for columns and wall is C30. The yield strength of steel reinforcement used is 410MPa. Fig. 19 presents the finite element model of the building structure, whose nonlinear equilibrium equations are typically solved by using numerical integration methods [70][71].

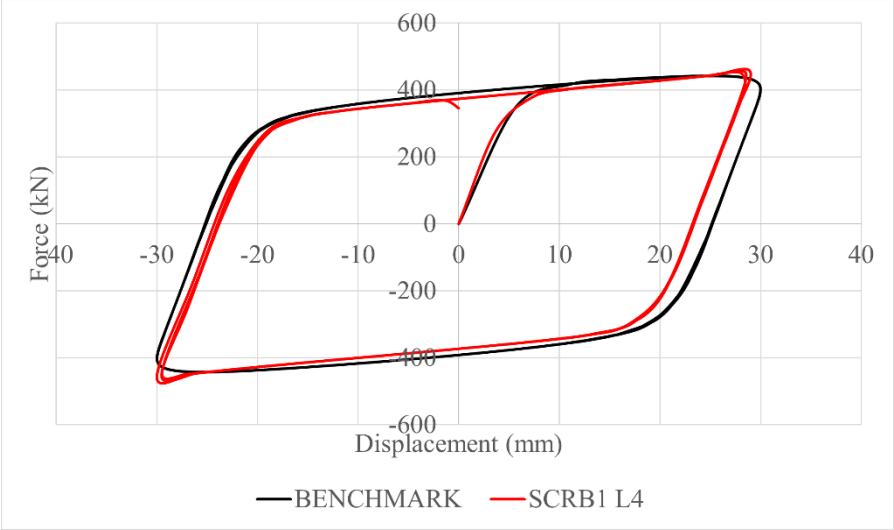

(a) SCRB1

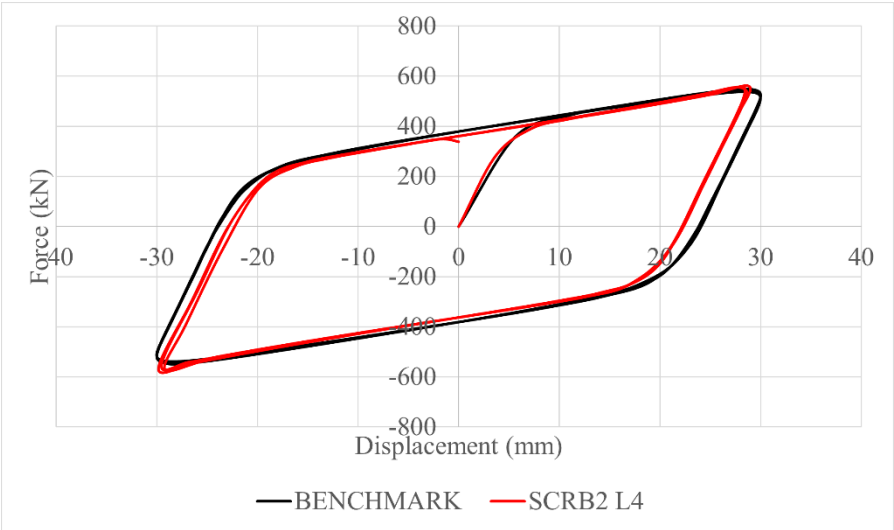

(b) SCRB2

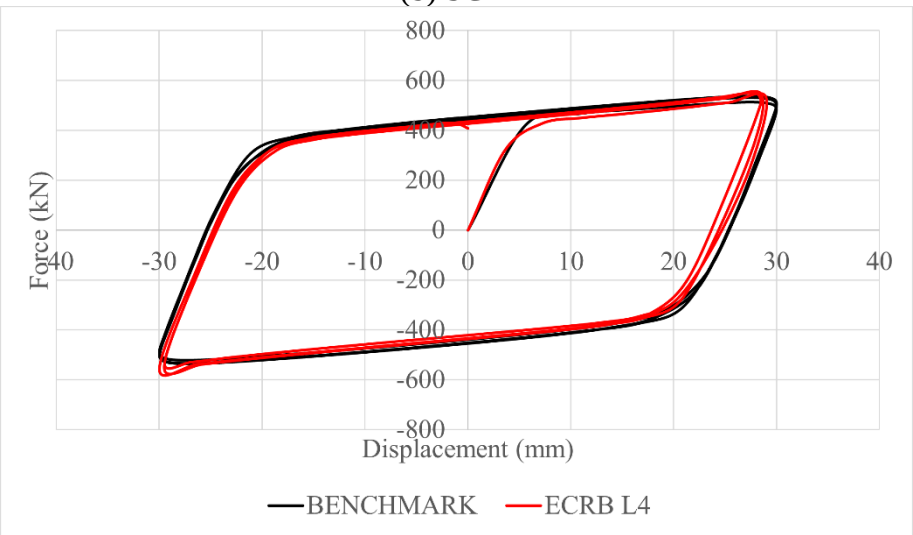

(c) ECRB

Fig. 13 Comparison of hysteresis curve from proposed bearings under simulation case L4 with benchmark case

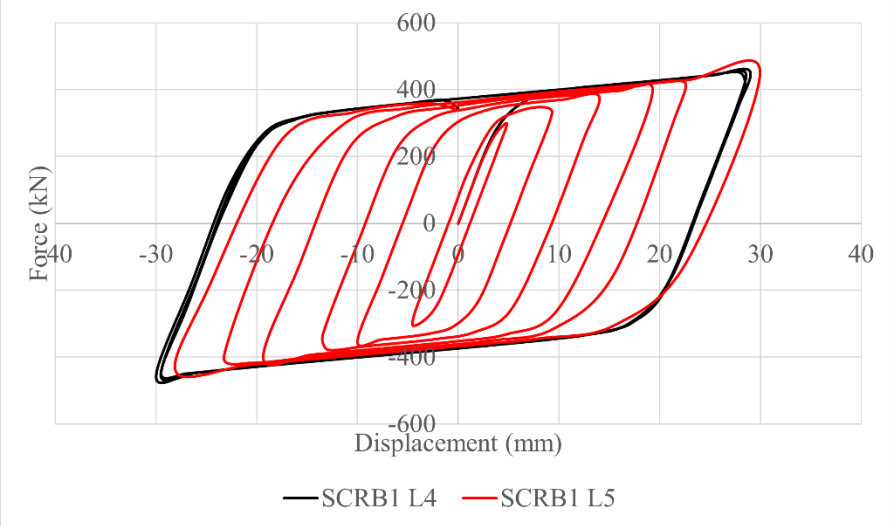

(a) SCRB1

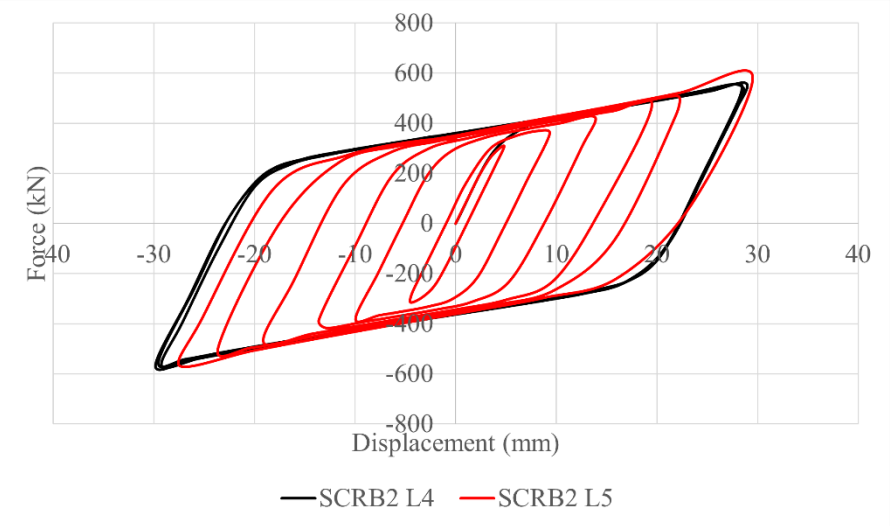

(b) SCRB2

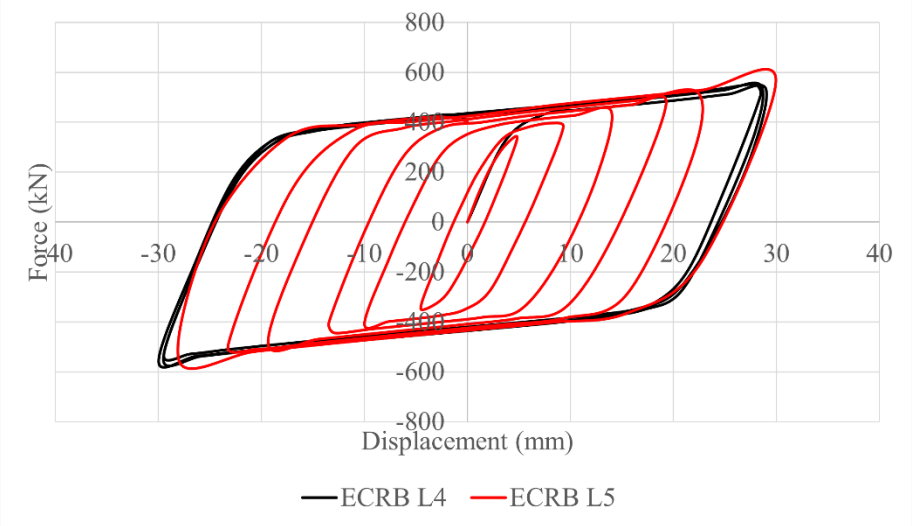

(c) ECRB

Fig. 14 Comparison of hysteresis curve from proposed bearings under simulation case L4 and L5

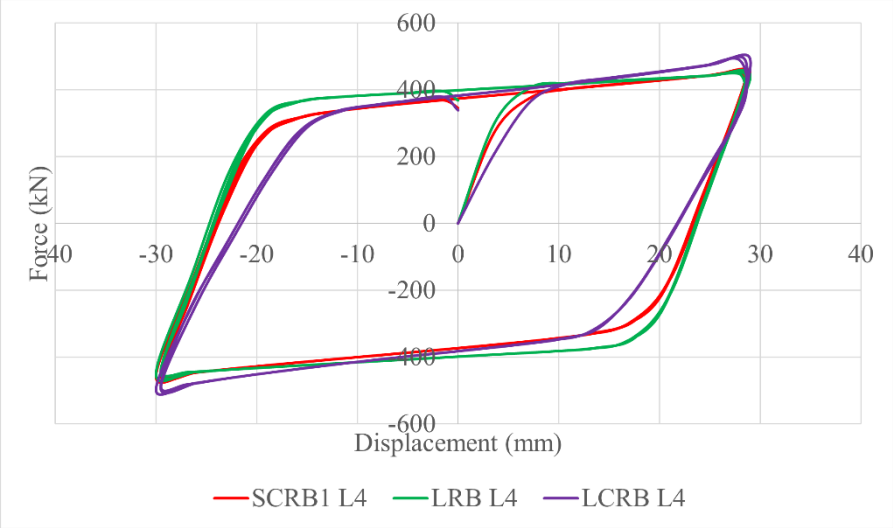

(a) SCRB1

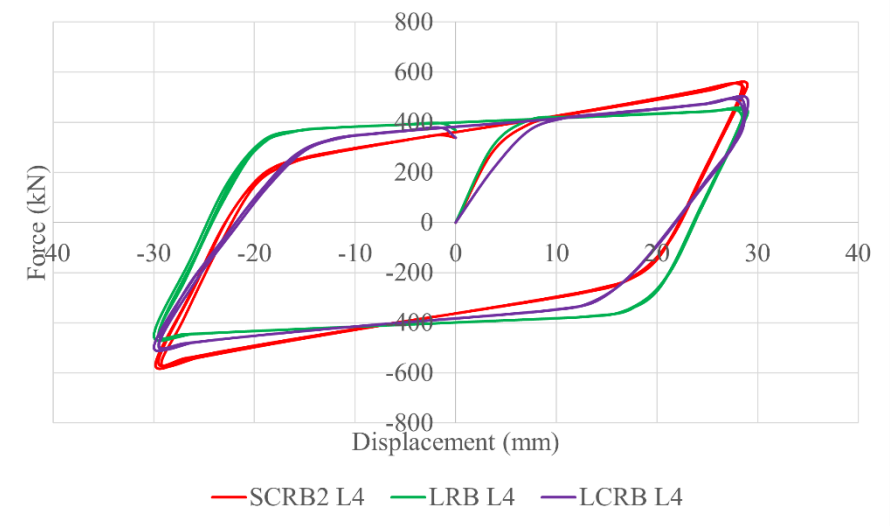

(b) SCRB2

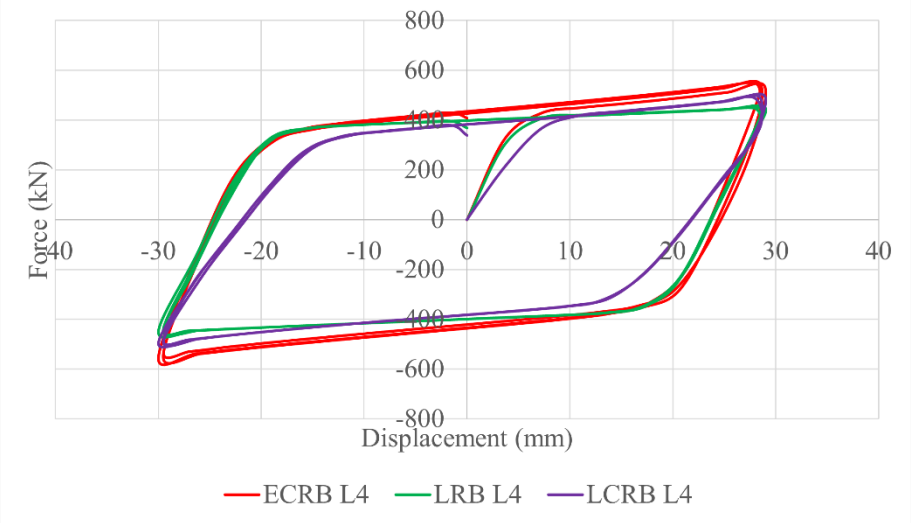

(c) ECRB

Fig. 15 Comparison of hysteresis curve from proposed bearings under simulation case L4 with LRB and LCRB

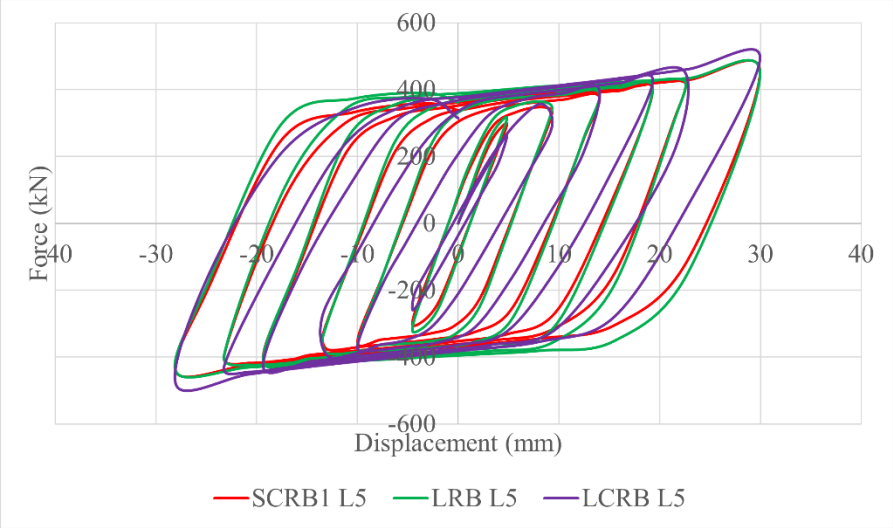

(a) SCRB1

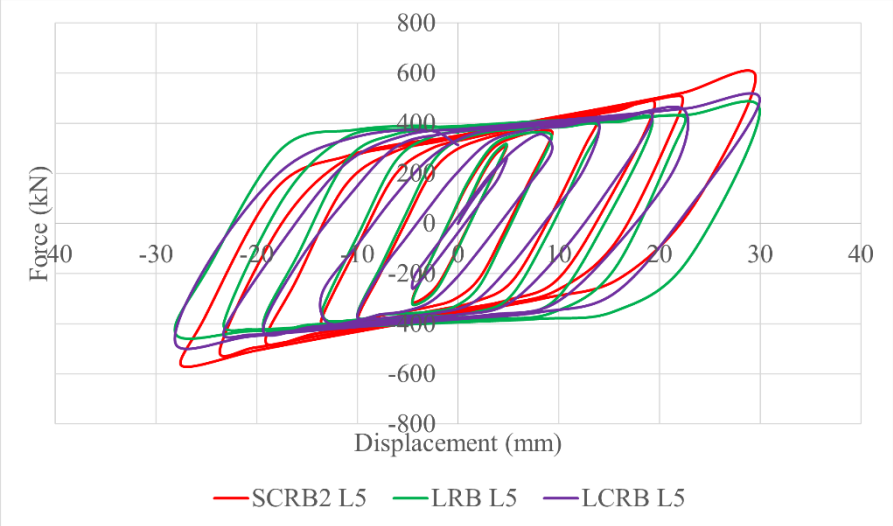

(b) SCRB2

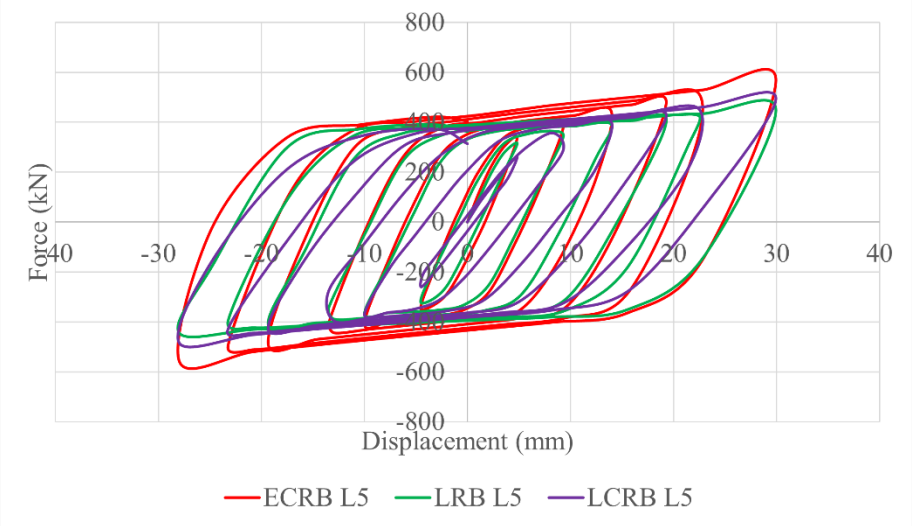

(c) ECRB

Fig. 16 Comparison of hysteresis curve from proposed bearings under simulation case L5 with LRB and LCRB

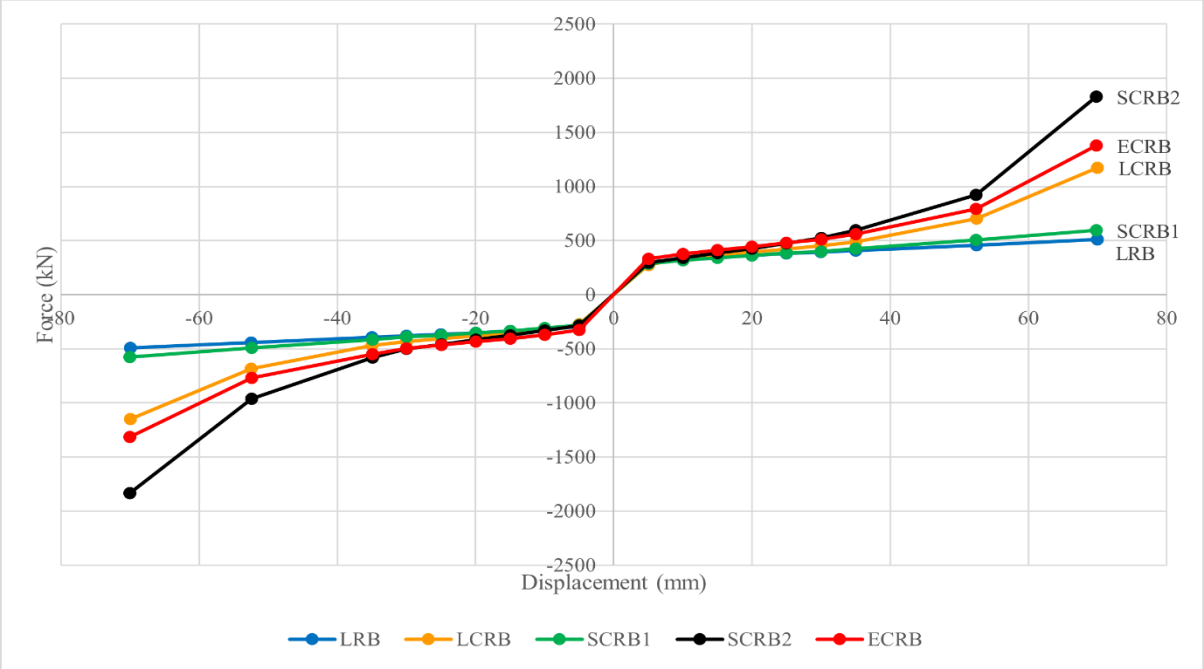

Fig. 17 Constitutive curve for bearings under various lateral strokes

7.2 Base isolators

Bearings are provided at 30 locations under the vertical structural members i.e. columns and wall to achieve base isolation. Six cases were simulated, where five of them were equipped with elastomeric bearings as base isolators, and the remaining one case simulated the fixed base condition as benchmark for performance comparison. Among the five elastomeric bearing, three of them were the bearings with proposed core-and-filler system i.e. SCRB1, SCRB2 and ECRB. Remaining two bearings were conventional elastomeric bearings that have been implemented in industry, namely laminated rubber bearing (LRB) and lead-core rubber bearing (LCRB).

In ETABS 2016, non-linear links were modelled at the base of vertical elements to simulate the base isolation. The behaviour of base isolators was described using spring and dashpot model. This analytical model consists of effective stiffness, k_{eff} and effective damping, c_{eff} [72]. The effective stiffness is taken as k_{eff} of elastomeric bearing obtained from cyclic shear test. Equivalent viscous damping, C_{eff} is used to calculate the effective damping component, as presented in Eq.(18), where the parameters are as defined in Fig. 7 [73]. The bearing characteristics from numerical simulation for design condition were used to derive the k and c components for elastomeric bearings. Table 12 shows the calculated k and c components for all elastomeric bearing.

$$C_{eff} = \frac{2}{\pi}\frac{ED}{(F_p - F_n)(d_p - d_n)} \tag{18}$$

Table 12 Effective stiffness and effective damping of elastomeric bearings

Bearing	$k = k_{eff}$ (kN/mm)	$c = C_{eff}$ (kNs/mm)
LRB	12.91	0.1522
LCRB	14.78	0.2459
SCRB1	13.32	0.2516
SCRB2	17.26	0.1952
ECRB	16.76	0.2366

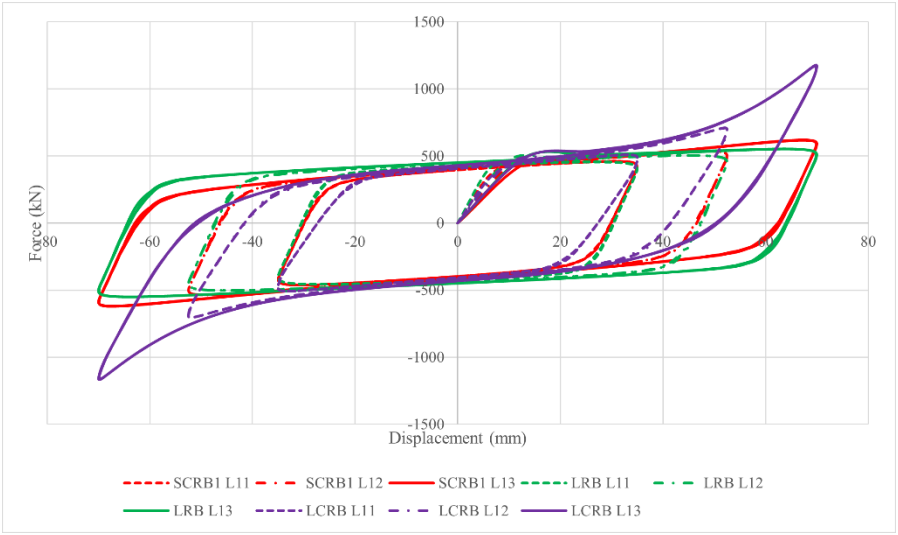

(a) SCRB1

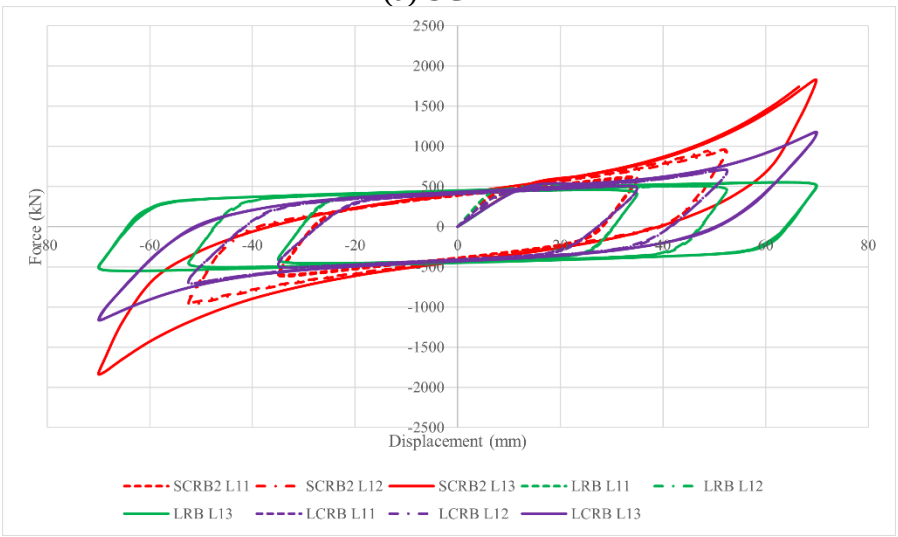

(b) SCRB2

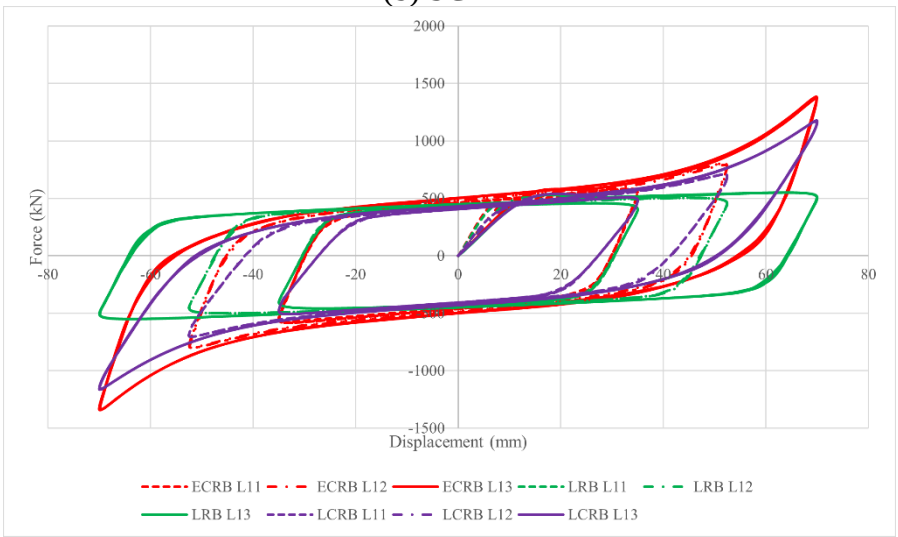

(c) ECRB

Fig. 18 Comparison of hysteresis curve from bearings under simulation case L11, L12 and L13

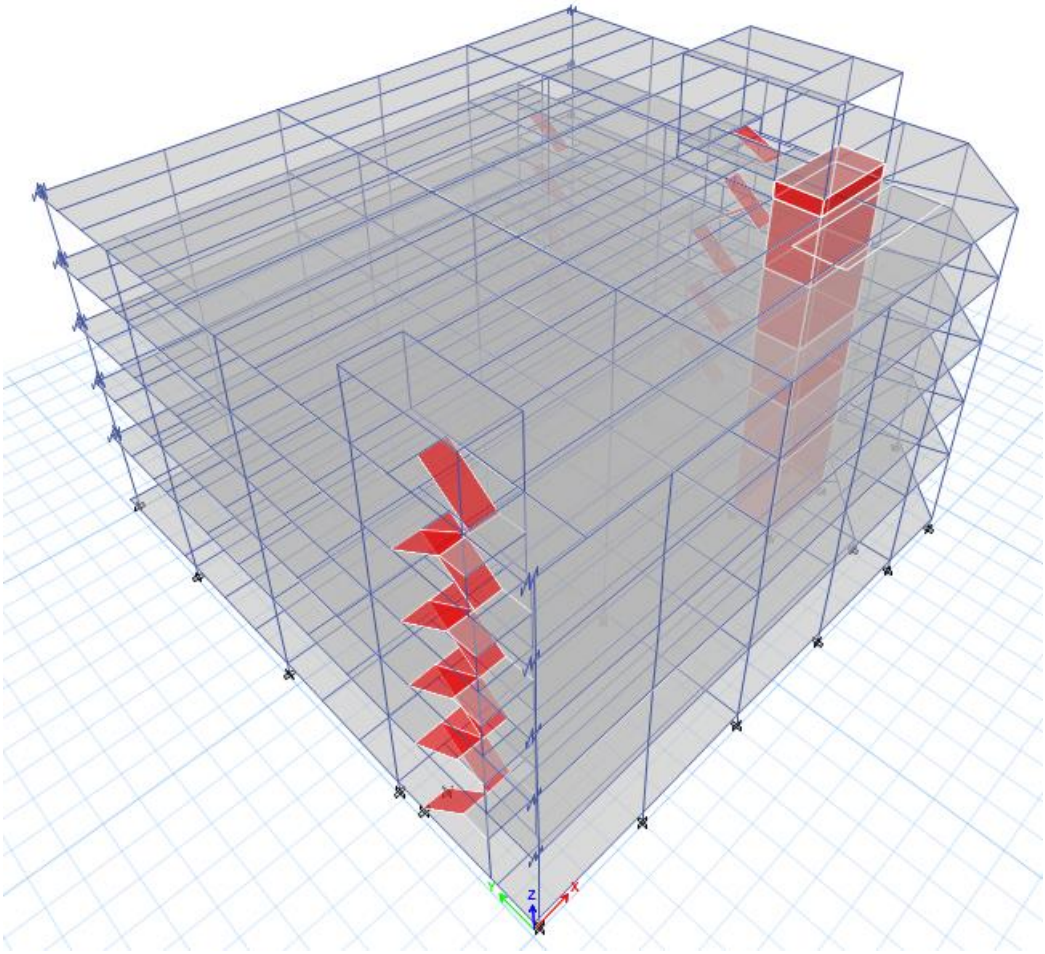

Fig. 19 Model of the studied 5-storey building structure

7.3 Time history analysis

The effective weight of structure for seismic analysis purpose is the sum of total dead load and 25% of total live load [74].

The nature of building structure is ordinary concrete moment-resisting frame, while the soil profile of the site is not available. The parameters associated with this type of building and site condition were determined for the construction of response spectrum, in accordance with ASCE 7-10 [75]. Spectral accelerations and long-period transition period T_L are dependent of the geographical location of site. In this study, the value of spectral acceleration for 0.2s and 1s, S_S and S_1 were conservatively assumed to produce the most critical design spectral acceleration value, while T_L is taken as 8s. Table 13 outlines the parameters determined as per ASCE 7-10.

Fig. 20 presents the target response spectrum under design-based earthquake (DBE) for the building structure based on the parameters determined as per ASCE 7-10. The probability of exceedance for DBE was 10% in 50 years, corresponding to return period of 475 years.

10 ground motion records were applied to the structure through nonlinear dynamic analysis, to obtain reliable seismic performance of building structure with and without base isolation [76]. The ground motion data were obtained from online database of Pacific Earthquake Engineering Research (PEER) centre. Table 14 lists the selected ground motion records for the analysis.

Table 13 Response spectrum parameters for the building structure as per ASCE 7-10

Parameter	Value	Reference
Diaphragm eccentricity	0.05	-
Approximate period parameters		
Ct	0.016	Table 12.8-2
x	0.09	Table 12.8-2
Response modification factor R	3	Table 12.2-1
Overstrength factor Q	3	Table 12.2-1
Deflection amplification factor Cd	2.5	Table 12.2-1
Risk category	II	Table 1.5-1
Importance factor I	1.0	Table 1.5-2
Site class	D	cl.11.4.2
Spectral acceleration		
For 0.2s, SS	0.25	-
For 1s, S1	0.1	-
Long-period transition period TL	8s	-
Site coefficients		
Fa	1.6	Table 11.4-1
Fv	2.4	Table 11.4-2
Design spectral acceleration		
For 0.2s, SDS	0.2667	-
For 1s, SD1	0.16	-
Damping ratio	5%	cl.16.1.3.1

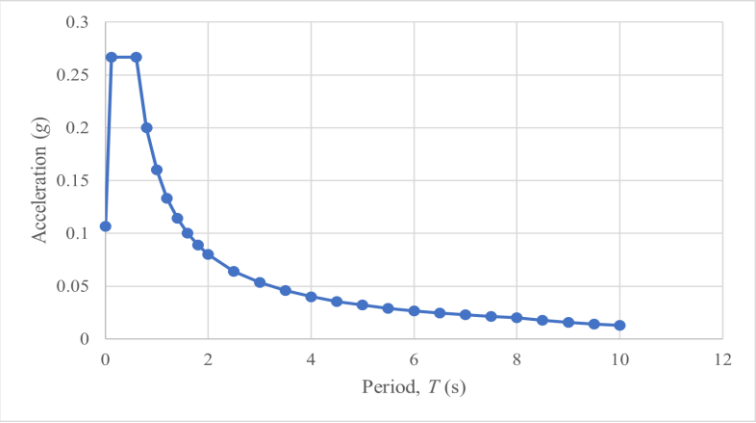

Fig. 20 Design response spectrum for the building as per ASCE 7-10

Table 14 Ground motion records implemented in this study

Record	Earthquake	Year	Station
RSN164	Imperial Valley – 06	1979	Cerro Prieto
RSN283	Irpina, Italy – 01	1980	Arienzo
RSN313	Corinth, Greece	1981	Corinth
RSN587	New Zealand – 02	1987	Matahina Dam
RSN727	Superstition Hills – 02	1987	Superstition Mtn Camera
RSN838	Landers	1992	Barstow
RSN1102	Kobe, Japan	1995	Chihaya
RSN1614	Duzce, Turkey	1999	Lamont 1061
RSN1633	Manjil, Iran	1990	Abbar
RSN1762	Hector Mine	1999	Amboy

The ground motion records were scaled to match the target response spectrum shown in Fig. 20. Considering the ductility of structure, the ground motions were then scaled by applying factor equivalent to *Ig/R*, in accordance with cl.16.1.4, ASCE 7-10 [77]. Orthogonal components of scaled ground motion were applied simultaneously to the structure in both x and y directions. P delta effect was taken into account during the nonlinear analysis.

Three main vibration mode, consisting of two translational about x and y directions, and one torsional about z axis were inspected. The fundamental mode of vibration is torsional, where its vibration period is 1.593s under fixed base condition. Torsional mode of vibration emerges as the fundamental mode of vibration due to the irregular and non-symmetrical arrangement of column and wall elements [78]. Refer to for the floor plan of building showing the irregular arrangement of vertical elements. The second and third mode of vibration are translational along y and x directions, with the period of 0.841s and 0.824s respectively. The elongation of period is observed all simulation cases that implement base isolation mechanism. The greatest period elongation occurs when LRB is implemented, with the period of 1.794s, 1.362s and 1.047s for first, second and third vibration mode respectively. On the other hand, the degree of period elongation by SCRB2 is the smallest compared to other base isolation cases. Table 15 presents the vibration modes and corresponding period under all six analysis cases.

Table 15 Period of vibration for the structure under six simulation cases

Base condition	Period (s)		
	First mode (torsional)	Second mode (translational - y)	Third mode (translational - x)
Fixed base	1.593	0.841	0.824
LRB	1.794	1.362	1.047
LCRB	1.788	1.348	1.041
SCRB1	1.791	1.353	1.043
SCRB2	1.784	1.335	1.036
ECRB	1.791	1.354	1.044

The implementation of base isolation system greatly reduces the base shear developed in building structure. Minimum 95% of reduction is observed from the analysis results. On the other hand, maximum storey drift for the cases with base isolation are generally greater than that for fixed base condition. Table 16 and Table 17 shows the maximum base shear developed throughout the ground motion period in x and y direction respectively. Fig. 22 demonstrates the maximum storey drift exhibited by structure during the simulation of ground motions.

Table 16 Maximum base shear developed in x direction for all cases

Ground motion	Maximum base shear in x direction (kN)					
	Fixed base	LRB	LCRB	SCRB1	SCRB2	ECRB
RSN164	1232.4	61.8	62.2	61.9	59.8	61.5
RSN283	1725.5	61.3	61.4	61.2	59.1	60.9
RSN313	1268.6	31.7	32.5	32.1	33.3	32
RSN587	1524.9	39.1	38.4	38.6	37.6	38.6
RSN727	1911.6	61.1	60.8	60.9	59.5	60.7
RSN838	1895.2	91.6	93.6	92.5	93	92.1
RSN1102	1705.6	72.6	74.8	73.9	75.7	73.6
RSN1614	1358.4	57.3	59.9	58.6	57.9	58
RSN1633	1347.6	49.8	50.4	50	49.2	49.7
RSN1762	1356.6	53.7	54.3	53.9	52.9	53.6

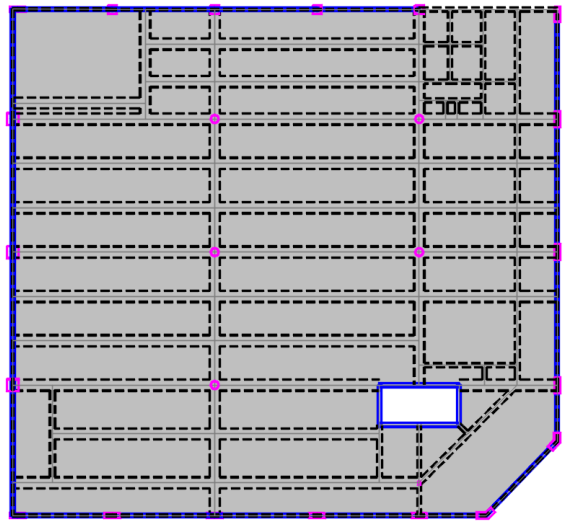

(a) Ground floor

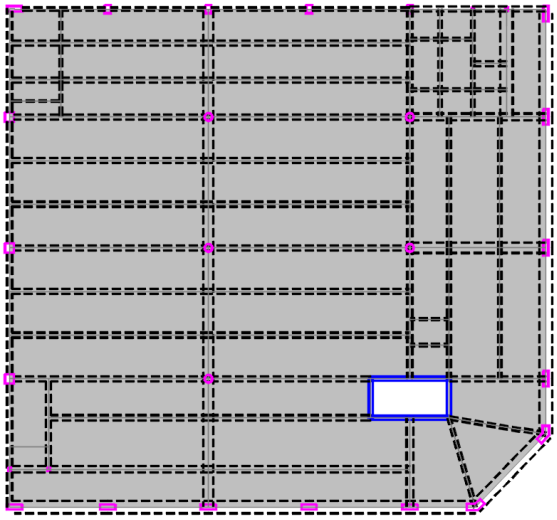

(b) Typical floor

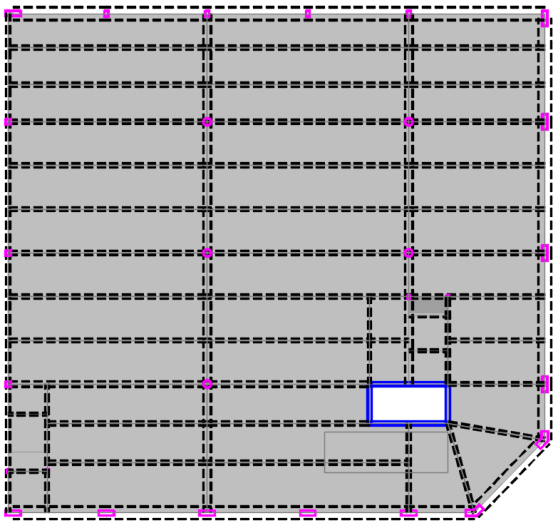

(c) Roof floor

COLUMN
WALL
BEAM

Fig. 21 Floor plan for the analysed building

Table 17 Maximum base shear developed in y direction for all cases

Ground motion	Maximum base shear in y direction (kN)					
	Fixed base	LRB	LCRB	SCRB1	SCRB2	ECRB
RSN164	2450.4	55.3	55.6	55.3	53.4	55
RSN283	2265.3	69.3	69.7	69.4	67.7	69
RSN313	2868.9	36.5	37.1	36.8	36.8	36.7
RSN587	2612.1	37.2	35.9	36.3	33.9	36.3
RSN727	1821.2	57.8	57.7	57.7	56.7	57.6
RSN838	1902.5	91.4	93.1	92.3	92.8	92
RSN1102	2200.0	67.7	69.8	68.9	70.7	68.7
RSN1614	1895.7	42.2	42.8	42.5	42.9	42.4
RSN1633	1663.7	45.7	45.6	45.5	43.6	45.2
RSN1762	1902.9	53	54.3	53.7	54.4	53.5

8.0 Discussions

8.1 Effect of sand properties

Based on the results shown for cases M1 to M8, the percentage of fluctuation in equivalent damping ratio and lateral stiffness of SCRB2 is 6.68 and 3.75 times higher than that occurs in SCRB1, respectively. In terms of dissipated energy, the percentage of fluctuation observed in SCRB2 is four times greater than that for SCRB1. However, the volume of sand used in SCRB2 is 1.88 times more than that for SCRB1. In other words, the effect of sand properties on the change in bearing characteristics is not solely due to the volume of sand in use. It is also a function of interfacial area between sand and bearing components, as well as the confinement state of sand mass. Under fully filled condition, the interfacial area is high, and the sand mass is in fully confined state. Having large interfacial contact area and being in fully confined state mean the sand mass completely transfers the stress developed upon displacement, subsequently fully deploy the resistance from other bearing components rather than absorb some of them via its own deformation. Both factors amplify the effect of sand properties variation on the degree of improvement or deterioration in terms of performance.

Despite large variability in the characteristics of SCRB2, it is still found to be a good replacement for lead in LCRB when it comes to improving the lateral stiffness of device. The value of k_{eff} for LCRB is 14.78kN/mm, and based on the findings in the present study, replacement of lead will only be deemed inefficient if and only if the sand filler is loosely packed, as simulated in case M1 and M2. On the other hand, the damping improves when the sand filler is loosely packed, as shown in M1 and M2, where the equivalent damping ratio achieved are 23.53% and 23.56%, with the difference of -4.3% when compared to that for LCRB (h_{eq} =24.59%).

In other words, by establishing medium to dense sand packing condition during manufacturing, the reduction in bearing stiffness due to material variability can be avoided. In return, the equivalent damping ratio of SCRB2 can be improved.

From the result for SCRB1 and SCRB2 shown in both Table 4 and Fig. 10, full height filler avoids the uneven stress distribution among the steel shims. The number of steel shims yielded in both SCRB2 and ECRB is less than that for LCRB. This indicates the use of stiffer steel core and full height filler successfully attracts the external forces, plays its role as main stiffness contributor of the bearing and reduces the stress in steel shims. Nonetheless, the stress developed in steel core is high and the yielding of core is anticipated throughout the operation period. This will increase the frequency of maintenance and replacement of steel core. As for

lead core, yielding does not invoke the concern for maintenance as lead can recrystallize under room temperature [6][7].
Further to the findings, the strength of lead in LCRB may deteriorate with increasing temperature due to hysteresis behaviour of lead itself. Over time, such deterioration may occur numerous times as the temperature threshold for deterioration is not very high [25]. On the other hand, quartz crystal structures in silica sand experiences changes when it is subjected to high temperature of 1000°C [79]. In other words, the resistance of sand particle may be considered indifferent to the temperature change throughout the bearing service life. In terms of the effect of temperature changes. yield stress of polymer decreases with increasing temperature. Based on a study conducted by Chen et al., yield stress of epoxy drops drastically when the temperature reaches 40°C [80]. The long-term performance of polymer is expected to deteriorate. This can be concluded from the creep and recovery behaviour of asphalt treated with epoxy, where the increase in permanent strain over long period of time is inevitable [56]. The main disadvantage of ECRB is the fluctuation of epoxy polymer filler under variation of temperature. When maintenance is required, the process may be troublesome as specific condition needs to be achieved before the polymer can be cured and ready for operation [80]. As for SCRB1 and SCRB2, the sand is susceptible to crushing due to the abrasion with steel components of the bearing. Nonetheless, the maintenance of SCRB1 and SCRB2 are easier than ECRB, where the replacement of sand filler does not require long procedure, and the bearing will be ready for operation afterwards [81].

8.2 Effect of loading conditions

High damping rubber is used for the bearings. For this reason, the hysteresis behaviour of bearings is sensitive to the velocity i.e. the frequency of lateral stroke. When subjected to high velocity, high damping force is induced and together with the stiffness force, the device develops high resistance against the applied loading. As a result, the magnitude of k_{eff} and Q becomes greater with increasing frequency. More work is done to stroke the bearing laterally and therefore, the ED increases with the frequency of loading as well. The reverse trend is observed in the equivalent damping ratio of LRB. This is because as the frequency increases from 0.0167Hz to 0.05Hz, the improvement in k_{eff} (+12.6%) surpasses that for ED (+10.5%) and based on the definition of h_{eq} shown in Eq. (15), the reduction of -1.8% is achieved.
While having the same amplitude, the k_{eff} for bearings subjected to loading in triangular displacement is greater than that obtained from sinusoidal displacement. Meanwhile, the reduction in ED is noticed at the same time. This phenomenon is related to the effect of loading frequency. For triangular displacement, the instantaneous velocity is consistent since the load function curve is straight. For sinusoidal displacement, the instantaneous velocity is the maximum at the beginning of cycle, and it reduces with increasing displacement. Based on calculation, the value of instantaneous velocity for sinusoidal displacement becomes less than that for triangular displacement when displacement of 23mm is attained (Fig. 23). As a result, when the lateral displacement surpasses 23mm, the corresponding lateral force magnitude becomes greater for triangular displacement, as presented in Fig. 24.
Moreover, when subjected to sudden change in loading direction as in triangular displacement, bearing device is forced to deploy its stiffness component immediately to tackle the inertia. Only after a while, damping component slowly plays its role and dissipates energy. Both are the contributing factors to lower h_{eq} and ED, and higher k_{eff}. For sinusoidal displacement, the instantaneous velocity at the beginning is the greatest and it decreases over time. Besides that, the rate of change of displacement is small as it approaches peak displacement, showing a smooth transition to the change in loading direction. The damping component of bearing device continues to stay active when the abrupt change in loading direction is less adverse.

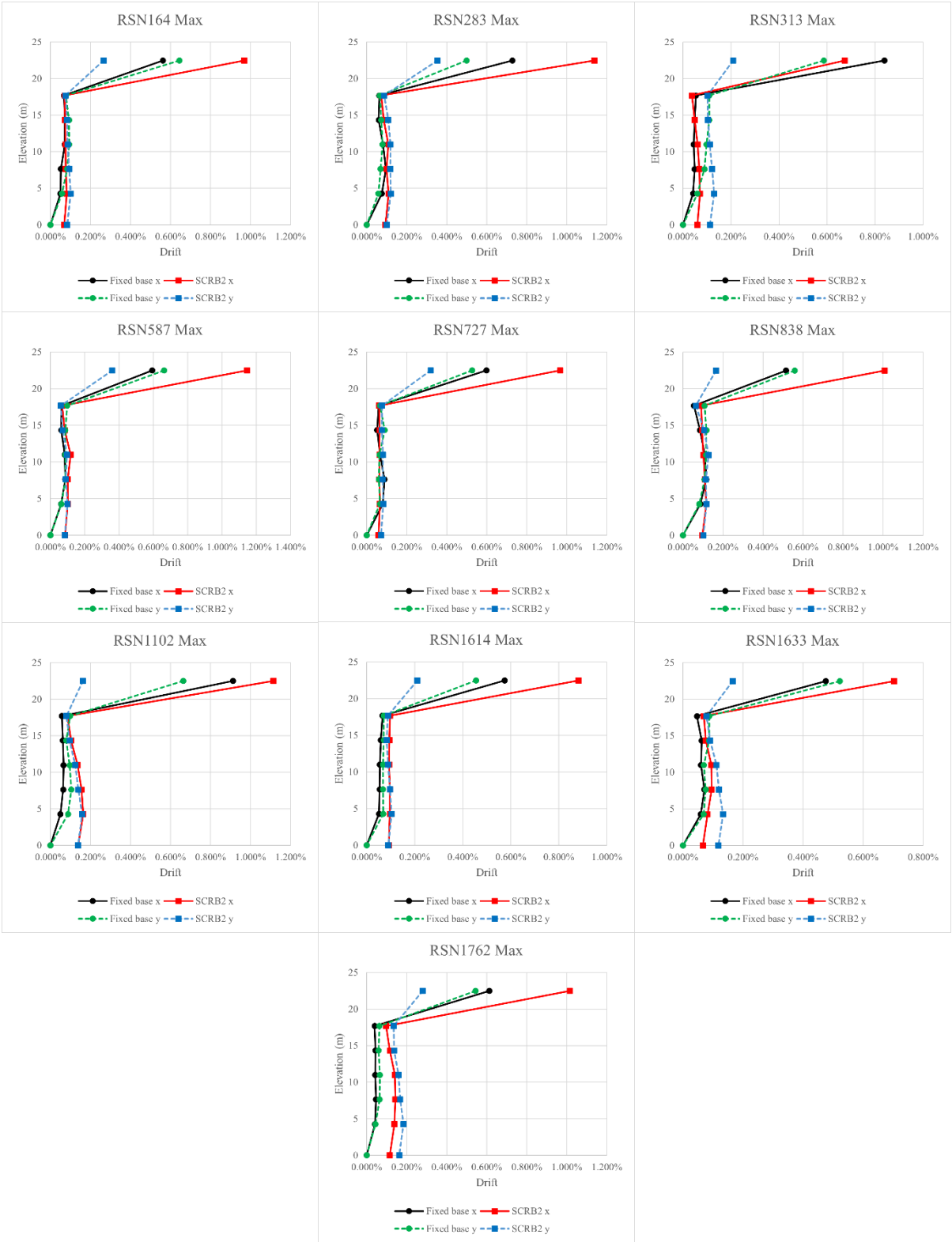

Fig. 22 Maximum storey drift attained throughout ground motion period for SCRB2

Despite subjected to more loading cycle and longer loading period (case L5), the k_{eff} of bearing is found greater than that for bearing subjected to three cycles of 30mm displacement (case L4). This behaviour is observed in all three types of bearings, indicating the characteristics of elastomeric bearing is mostly governed by the most critical lateral displacement attained over the loading history. When the deformation of elastomeric bearing over the history is large,

rubber is stretched and h_{eq} increases due to the softening. On the other hand, the softened rubber possesses inferior strength compared to its original state. As a result, k_{eff} reduced in the wake of increment in h_{eq}.

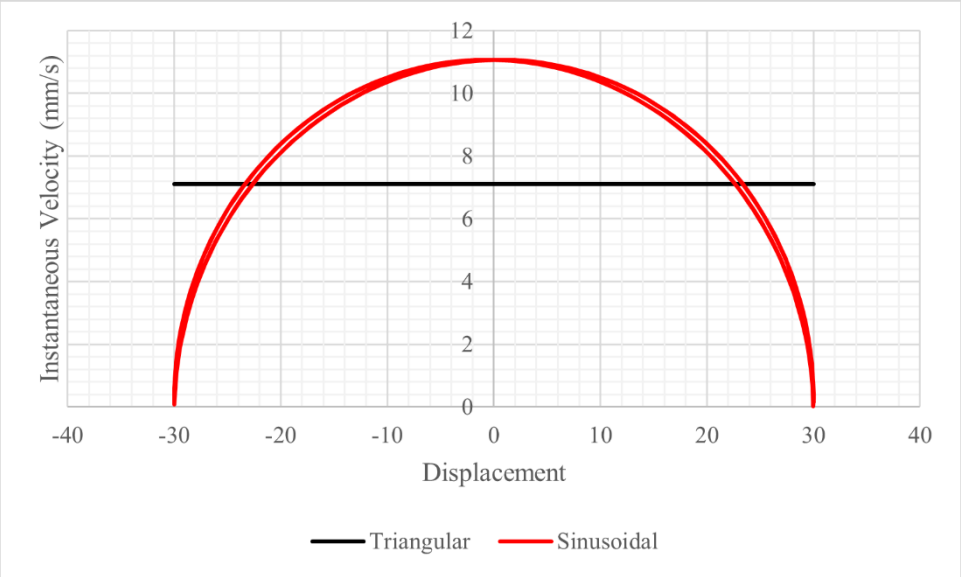

Fig. 23 Comparison of instantaneous velocity of sinusoidal and triangular displacement under various displacement

The finding for LCRB under case L4 and L5 is consistent with literature, as mentioned by Ozdemir & Dicleli where the temperature rise in lead core can be reduced by using smaller cyclic displacement amplitude. When the rise in temperature is less, the deterioration of lead core strength is small [82]. As a result, the strength of LCRB is higher if it has not been subjected to large displacement before, as observed by comparing the results from L4 and L5. The properties of LCRB are correlated to loading history [82], and from the present study, the effect of loading history is found more prominent in LCRB than other bearings. Thus, the behaviour of lead is more sensitive to loading history, compared to steel, sand, epoxy and rubber.

The constitutive curves for SCRB2 and ECRB are trilinear, where the piecewise points of three linear segment are 5mm and 52.5mm, equivalent to 14.28% and 150% shear strain. For SCRB1, the constitutive curve is bilinear, and the slope of curve reduced after 14.28% shear strain.

Before the bearings reach 14.28% shear strain, its stiffness is high, indicating greater resistance from undeformed rubber and filler. When shear strain exceeds 14.28%, the resistance is reduced as the deformation of rubber and filler becomes more and more significant. This can be seen from milder slope of segment on the constitutive curve between 14.28% and 150% shear strain. When 150% shear strain is achieved, the resistance increases significantly. Under fully filled condition, as the space between steel core and elastomeric bearing body reduces, the filler material in between is highly stressed and squeezed. Greater force is required to push the bearing at this point, as the sand particles or molecules of epoxy are tightly packed and leave little room for further compression. Similar phenomenon is observed for LCRB, and this is consistent with the findings presented by Kim et al., where the corresponding lateral force increased drastically at some point when it is being tested with varying shear strains [83].

For SCRB1 on the other hand, this phenomenon is not observed since the sand filler is not confined and therefore, the particles are free to displace away from the high stress region, and intense compression is thus less likely to occur in this region.

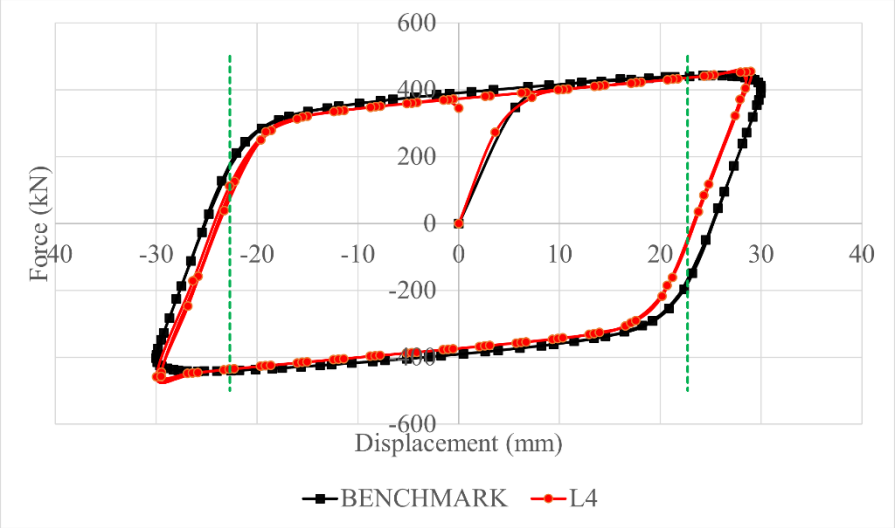

(a) SCRB1

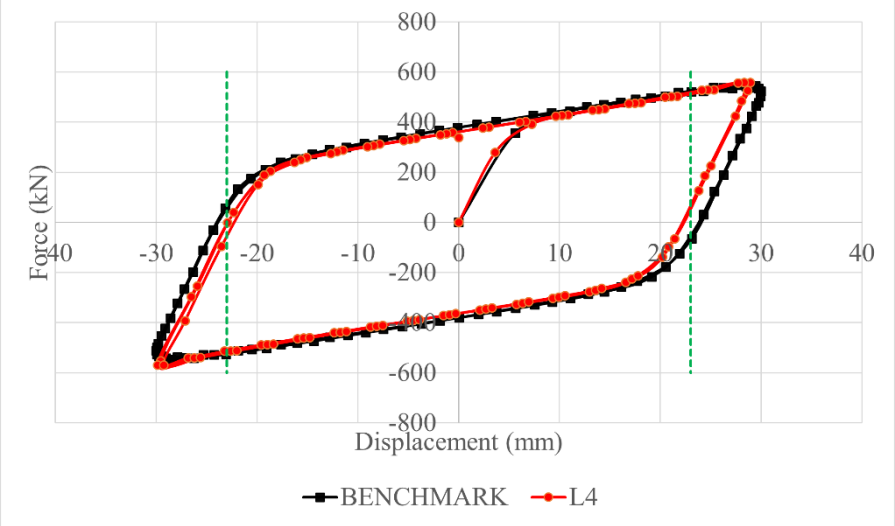

(b) SCRB2

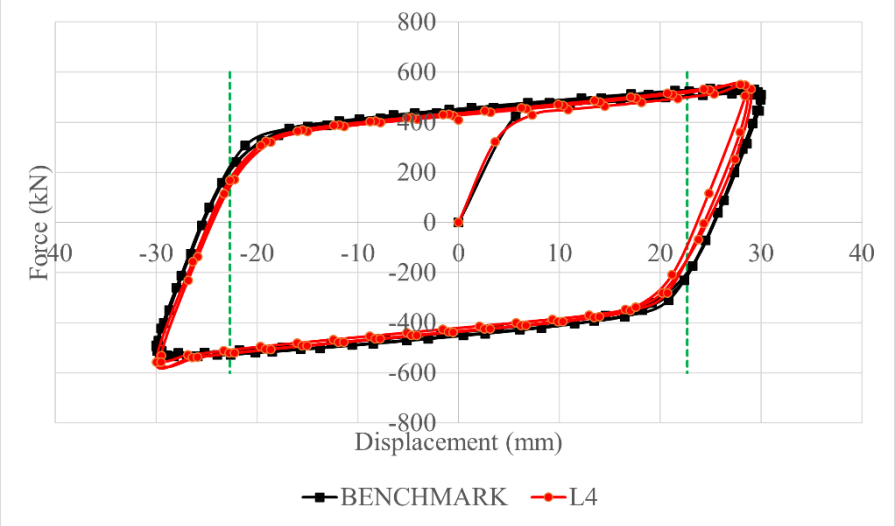

(c) ECRB

Fig. 24 Change in the lateral force for case L4 before and after the transition displacement

8.3 Performance of elastomeric bearing as base isolator in structure

The implementation of elastomeric bearing successfully elongates the vibration period of structure. By permitting the movement of superstructure at base level, the stiffness of structure is reduced, and this causes the increase its vibration period. By elongating the vibration period, pseudo spectral acceleration applied on structure is reduced. When pseudo spectral acceleration is reduced, the force developed in structure during ground motion can be reduced. In addition, the base isolator deforms with ground motion and reduces the forces transferred to superstructure. With these combined effects, the base shear of structure is drastically reduced by at least 95% when comparing to benchmark fixed base condition. The trade-off of this improvement is larger storey drift.

By comparing the structural response after implementing all types of elastomeric bearings, their differences are found negligible. This shows the superiority of any bearing against each other diminishes as the devices are now only a small part in the structural system. Nevertheless, the difference is still noticeable where SCRB2 shows the minimum elongation of period when compared to other bearings, while having the highest effective stiffness compared to other bearings.

From this study, the application of proposed elastomeric bearing in structure is as effective as conventional bearings i.e. LRB and LCRB. The proposed core-and-filler mechanism is better than LCRB in term of durability, and to LRB in term of the ability to provide exponentially large stiffness against excessive displacement. For these reasons, the elastomeric bearing utilizing the proposed core-and-filler mechanism is deemed an effective alternative to conventional LRB and LCRB.

9.0 Conclusions

In this study, a new rubber elastomer bearing with steel core and filler system consists of granular or polymer filler is developed as an alternative system to lead core bearing isolators. The pure sand is implemented as granular filler and epoxy is used as polymer filler.

Accordingly, the special design process for the proposed elastomeric bearing under applied load is developed. The procedure integrates the current implemented code of practice and produces elastomeric bearing details that does not only satisfy the design standard, but also compatible with the implementation of core-and-filler system.

Finite element model for rubber bearings for three types of proposed core-and-filler mechanisms were developed. Thereafter, the parametric study is conducted to explore the influence of sand properties on the performance of rubber bearing with partially and fully sand filler. Also, the effect of material variability is explicitly studied by comparison the behaviour of bearing with lead rubber bearing, for further insight on the effectiveness of lead material replacement. Besides that, the correlation between performance and loading conditions in terms of loading frequency, displacement pattern and applied displacement were studied.

From result of this study, the following findings are drawn and summarized:

1. Among the elastomeric bearings, the addition of lead core and proposed core-and-filler system in conventional bearing causes the improvement in effective damping. The improvement brought forth by LCRB is 61.6% compared to LRB. Among the bearing with core-and-filler mechanism, SCRB1 showed the best isolation performance with 25.16% equivalent damping, achieve an improvement of 2.32% when compared to LCRB. This value is also 28.9% and 6.3% greater than the equivalent damping ratio calculated for SCRB2 and ECRB. Comparing to LCRB, the damping of both SCRB2 and ECRB are inferior (-20.6% and -3.8% respectively).
2. Conversely, SCRB2 was found possessing superior effective stiffness, in which by replacing lead core with fully filled sand and core system, effective stiffness increased by

16.8%. Such stiffness was 3% higher than effective stiffness for ECRB, and 29.6% greater when compared to SCRB1. Meanwhile, the introduction of such system in conventional bearing improves the stiffness by 33.7%.

3. For the rubber bearing with full sand, the filler packing condition can be manipulated during manufacturing stage to produce intended improvement after replacing lead core. By reducing the sand filler volume, improvement up to 32.9% can be achieved in terms of damping, as exhibited from SCRB2 benchmark case to SCRB1 case M1. By changing fully filled sand filler to densely packed condition, improvement of 18.3% in terms of effective stiffness is possible. Thus, the variability of sand properties due to various reasons does not compromise the effectiveness of system comprising steel core and full sand filler in SCRB2 to replace the lead core in LCRB.
4. For elastomeric bearing with sand core-and-filler mechanism, the damping can be improved by reducing the modulus of elasticity of sand, while the stiffness can be improved by increasing it. The effectiveness in the improvement by changing the modulus of elasticity of sand is dictated by the volume of used sand filler, filler confinement state and interfacial area between sand and bearing components. This is observed for SCRB2, where the improvement in damping can be increased by 20.7% by changing the sand packing condition from dense to loose, and 15.5% in stiffness by changing the sand packing condition from loose to dense. Relatively, the maximum improvement of merely 3.1% and 4% for damping and stiffness is seen in SCRB1.
5. The constitutive curve of elastomeric bearings with fully filled void i.e. SCRB2 and ECRB is trilinear, where the steel core functions as displacement control system when large strain occurs, and it is maximized when the filler is confined and forced to resist the exerted loading. On the other hand, the constitutive curve for SCRB1 is bilinear, where the sand particles tend to move elsewhere when stressed, and unable to fully utilize the function of steel core.
6. The proposed core-and-filler system with fully filled sand emerges as a strong alternative for conventional LRB and LCRB bearings for its noticeable improvement in bearing strength.

Declaration of Competing Interest

The authors declare that they have no known competing financial interests or personal relationships that could have appeared to influence the work reported in this paper.

References

[1] Clemente P, Bongiovanni G, Buffarini G, Saitta F, Castellano MG, Scafati F. Effectiveness of HDRB isolation systems under low energy earthquakes. Soil Dynamics and Earthquake Engineering 2019; 118: 207–220. https://doi.org/10.1016/j.soildyn.2018.12.018.

[2] Chaudhary MTA, Abé M, Fujino Y. Performance evaluation of base-isolated Yama-agé bridge with high damping rubber bearings using recorded seismic data. Engineering Structures 2001; 23(8): 902–910. https://doi.org/10.1016/S0141-0296(00)00117-6.

[3] Markou AA, Manolis GD. Mechanical models for shear behavior in high damping rubber bearings. Soil Dynamics and Earthquake Engineering 2016; 90: 221–226. http://doi.org/10.1016/j.soildyn.2016.08.035.

[4] Marano GC, Greco R. Effciency of base isolation systems in structural seismic protection and energetic assessment. Earthquake Engineering & Structural Dynamics 2003; 32(10): 1505-1531, 2003. https://doi.org/10.1002/eqe.286.

[5] Cardone D, Gesualdi G, Nigro D. Effects of air temperature on the cyclic behavior of elastomeric seismic isolators. Bulletin of Earthquake Engineering 2011; 9(4): 1227–1255. https://doi.org/10.1007/s10518-011-9244-8.
[6] Robinson WH. Lead-rubber hysteretic bearings suitable for protecting structures during earthquakes. Earthquake Engineering & Structural Dynamics 1982; 10(4): 593–604. https://doi.org/10.1002/eqe.4290100408.
[7] Robinson WH, Tucker AG. Test results for lead-rubber bearings for WM. Clayton building, Toe Toe bridge and Waiotukupuna bridge. Bulletin of the New Zealand National Society for Earthquake Engineering 1981; 14(1): 21-33.
[8] Kang BS, Li L, Ku TW. Dynamic response characteristics of seismic isolation systems for building structures. Journal of Mechanical Science and Technology 2009; 23(8): 2179–2192. https://doi.org/10.1007/s12206-009-0437-x.
[9] Losanno D, Spizzuoco M, Calabrese A. Bidirectional shaking-table tests of unbonded recycled-rubber fiber-reinforced bearings (RR-FRBs). Structural Control and Health Monitoring 2019: 26; e2386. https://doi.org/10.1002/stc.2386
[10] Matsushita H, Fujisawa K, Sasaki T. Development of peripherally restraining type seismic isolator. SMiRT-12 1993; K25/4: 375-380.
[11] Li H, Tian S, Dang X, Yuan W, Wei K. Performance of steel mesh reinforced elastomeric isolation bearing: Experimental study. Construction and Building Materials 2016; 121: 60–68. http://doi.org/10.1016/j.conbuildmat.2016.05.143.
[12] Choi E, Nam T, Cho BS. A new concept of isolation bearings for highway steel bridges using shape memory alloys. Canadian Journal of Civil Engineering 2005; 32(5): 957–967. https://doi.org/10.1139/l05-049.
[13] Dezfuli FH, Alam M S. Performance-based assessment and design of FRP-based high damping rubber bearing incorporated with shape memory alloy wires. Engineering Structures 2014; 61: 166–183. https://doi.org/10.1016/j.engstruct.2014.01.008.
[14] Tan KC, Hejazi F. Esfahani HM, Chong T. Development of elastomeric rubber bearing utilizing core-and-filler system. Structures 2022; 37: 125-139. https://doi.org/10.1016/j.istruc.2021.12.074
[15] Jangid RS, Kelly JM. Base isolation for near-fault motions. Earthquake Engineering & Structural Dynamics 2001; 30(5): 691-707. https://doi.org/10.1002/eqe.31.
[16] Kim SH, Mha HS, Lee SW. Effects of bearing damage upon seismic behaviors of a multi-span girder bridge. Engineering Structures 2006; 28(7): 1071–1080. https://doi.org/10.1016/j.engstruct.2005.11.015.
[17] Gottesfield P, Were FH, Adogame L, Gharbi S, San D, Nota MM, Kuepouo G. Soil contamination from lead battery manufacturing and recycling in seven African countries. Environmental Research 2018; 161: 609–614 https://doi.org/10.1016/j.envres.2017.11.055.
[18] Gałuszka A, Migaszewski ZM, Dołęgowska S, Michalik A. Geochemical anomalies of trace elements in unremediated soils of Mt. Karczówka, a historic lead mining area in the city of Kielce, Poland. Science of Total Environment 2018; 639: 397–405. https://doi.org/10.1016/j.scitotenv.2018.05.174.
[19] Bose-O'Reilly S, Yabe J, Makumba J, Schutzmeier P, Ericson B, Caravanos J. Lead intoxicated children in Kabwe, Zambia. Environmental Research 2018; 165: 420–424. https://doi.org/10.1016/j.envres.2017.10.024.
[20] Clay K, Portnykh M, Severnini E. The legacy lead deposition in soils and its impact on cognitive function in preschool-aged children in the United States. Economics & Human Biology 2019; 33: 181-192. https://doi.org/10.1016/j.ehb.2019.03.001.

[21] Burtscher SL, Dorfmann A. Compression and shear tests of anisotropic high damping rubber bearings. Engineering Structures 2004; 26(13): 1979–1991. https://doi.org/10.1016/j.engstruct.2004.07.014.
[22] Montuori GM, Mele E, Marrazzo G, Brandonisio G, De Luca A. Stability issues and pressure–shear interaction in elastomeric bearings: The primary role of the secondary shape factor. Bulletin of Earthquake Engineering 2016; 14(2): 569–597. https://doi.org/10.1007/s10518-015-9819-x.
[23] Gauron O, Saidou A, Busson A, Siqueira GH, Paultre P. Experimental determination of the lateral stability and shear failure limit states of bridge rubber bearings. Engineering Structures 2018; 174: 39–48. https://doi.org/10.1016/j.engstruct.2018.07.039.
[24] Choun YS, Park J, Choi IK. Effects of mechanical property variability in lead rubber bearings on the response of seismic isolation system for different ground motions. Nuclear Engineering and Technology 2014; 46(5): 605–618. http://doi.org/10.5516/NET.09.2014.718.
[25] Ahmadipour M, Alam MS. Sensitivity analysis on mechanical characteristics of lead-core steel-reinforced elastomeric bearings under cyclic loading. Engineering Structures 2017; 140: 39–50. http://doi.org/10.1016/j.engstruct.2017.02.014.
[26] Rahnavard R, Thomas RJ. Numerical evaluation of steel-rubber isolator with single and multiple rubber cores. Engineering Structures 2019; 198: 109532. https://doi.org/10.1016/j.engstruct.2019.109532.
[27] Russo G, Pauletta M. Sliding instability of fiber-reinforced elastomeric isolators in unbonded applications. Engineering Structures 2013; 48: 70–80. http://doi.org/10.1016/j.engstruct.2012.08.031.
[28] Madera Sierra IE, Losanno D, Strano S, Marulanda J, Thomson P. Development and experimental behavior of HDR seismic isolators for low-rise residential buildings. Engineering Structures 2019; 183: 894–906. https://doi.org/10.1016/j.engstruct.2019.01.037.
[29] Strauss A, Apostolidi E, Zimmermann T, Gerhaher U, Dritsos S. Experimental investigations of fiber and steel reinforced elastomeric bearings: Shear modulus and damping coefficient. Engineering Structures 2014; 75: 402–413. http://doi.org/10.1016/j.engstruct.2014.06.008.
[30] Pauletta M, Cortesia A, Russo G. Roll-out instability of small size fiber-reinforced elastomeric isolators in unbonded applications. Engineering Structures 2015; 102: 358–368. http://doi.org/10.1016/j.engstruct.2015.08.019.
[31] Vaiana N, Losanno D, Ravichandran N. A novel family of multiple springs models suitable for biaxial rate-independent hysteretic behavior. Computers & Structures 2021: 244; 106403. https://doi.org/10.1016/j.compstruc.2020.106403
[32] Vaiana N, Sessa S, Marmo F, Rosati L. An accurate and computationally efficient uniaxial phenomenological model for steel and fiber reinforced elastomeric bearings. Composite Structures 2019: 211; 196-212. https://doi.org/10.1016/j.compstruct.2018.12.017
[33] Bradley GL, Chang PC, Mckenna GB. Rubber modelling using uniaxial test data. Journal of Applied Polymer Science 2001; 81(4): 837-848. https://doi.org/10.1002/app.1503.
[34] Treloar LRG. Stress-strain data for vulcanised rubber under various types of deformation. Transactions of the Faraday Society 1944; 40: 59-70. https://doi.org/10.1039/TF9444000059.
[35] Rivlin RS, Saunders DW. Large elastic deformations of isotropic materials VII. Experiments on the deformation of rubber. Philosophical Transactions of the Royal Society A 1951; 243(865): 251-288. https://doi.org/10.1098/rsta.1951.0004.

[36] Jones DF, Treloar LRG. The properties of rubber in pure homogeneous strain. Journal of Physics D: Applied Physics 1975; 8: 1285-1304. https://doi.org/10.1088/0022-3727/8/11/007.
[37] Vangerko H, Treloar LRG. The inflation and extension of rubber tube for biaxial strain studies. Journal of Physics D: Applied Physics 1978; 11: 1969-1978. https://doi.org/10.1088/0022-3727/11/14/009.
[38] Ogden RW. Large deformation isotropic elasticity – on the correlation of theory and experiment for incompressible rubberlike solids. Proceedings of the Royal Society of London A. 1972; 326: 565-584.
[39] Arruda EM, Boyce MC. A three-dimensional constitutive model for the large stretch behavior of rubber elastic materials. Journal of the Mechanics and Physics of Solids 1993; 41(2): 389-412. https://doi.org/10.1016/0022-5096(93)90013-6.
[40] Caroll MM. A strain energy function for vulcanized rubbers. Journal of Elasticity 2011; 103: 173-187. https://doi.org/10.1007/s10659-010-9279-0.
[41] Warn GP, Weisman J. Parametric finite element investigation of the critical load capacity of elastomeric strip bearings. Engineering Structures 2011; 33(12): 3509–3515. http://doi.org/10.1016/j.engstruct.2011.07.013.
[42] Steinmann, P., Hossain, M. & Possart, G., "Hyperelastic models for rubber-like materials: Consistent tangent operators and suitability for Treloar's data," *Archive of Applied Mechanics*, vol. 82, no. 9, pp.1183-1217, 2012. https://doi.org/10.1007/s00419-012-0610-z
[43] Zhou T, Wu YF, Li AQ. Numerical study on the ultimate behavior of elastomeric bearings under combined compression and shear. KSCE Journal of Civil Engineering 2018; 22(9): 3556–3566. https://doi.org/10.1007/s12205-018-0949-y.
[44] Kalfas KN, Mitoulis SA, Katakalos K. Numerical study on the response of steel-laminated elastomeric bearings subjected to variable axial loads and development of local tensile stresses. Engineering Structures 2017; 134: 346–357. http://doi.org/10.1016/j.engstruct.2016.12.015.
[45] Cundall PA, Strack ODL. The discrete numerical model for granular assemblies. Geotechnique 1979; 29(1): 47-65. https://doi.org/10.1680/geot.1979.29.1.47.
[46] Belheine N, Plassiard JP, Donze FV, Darve F, Seridi A. Numerical simulation of drained triaxial test using 3D discrete element modelling. Computers and Geotechnics 2009; 36(1-2): 320-331. https://doi.org/10.1016/j.compgeo.2008.02.003.
[47] Yan Y, Ji S. Discrete element modeling of direct shear tests for a granular material. International Journal for Numerical and Analytical Methods in Geomechanics 2010; 34(9): 978-990. https://doi.org/10.1002/nag.848.
[48] Lim KW, Andrade JE. Granular element method for three-dimensional discrete element calculations. International Journal for Numerical and Analytical Methods in Geomechanics 2014; 38(2): 167-188. https://doi.org/10.1002/nag.2203.
[49] Kawamoto R, Ando E, Viggiani G, Andrade JE. Level set discrete element method for three-dimensional computations with triaxial case study. Journal of the Mechanics and Physics of Solids 2016; 91: 1-13. https://doi.org/10.1016/j.jmps.2016.02.021.
[50] Tong L, Wang YH. DEM simulations of shear modulus and damping ratio of sand with emphasis on the effects of particle number, particle shape, and aging. Acta Geotechnica 2015; 10: 117-130. https://doi.org/10.1007/s11440-014-0331-2.
[51] Ai J, Chen JF, Ooi JY. Finite element simulation of the pressure dip in sandpiles. International Journal of Solids and Structures 2013; 50: 981-995. https://dx.doi.org/10.1016/j.ijsolstr.2012.12.006.
[52] Chang WJ, Phantachang T. Effects of gravel content on shear resistance of gravelly soils. Engineering Geology 2016; 207: 78-90. http://doi.org/10.1016/j.enggeo.2016.04.015.

[53] Wei Y, Yang Y, Tao M. Effects of gravel content and particle size on abrasivity of sandy gravel mixture. Engineering Geology 2018; 243: 26-35. https://doi.org/10.1016/j.enggeo.2018.06.009.
[54] Weibull W. A statistical distribution function of wide applicablility. Journal of Applied Mechanics 1951; 18: 293-297.
[55] Zhang K, Wang L, Wang F, Wang G, Li Z. Preparation and characterization of modified-clay-reinforced and toughened epoxy-resin nanocomposites. Journal of Applied Polymer Science 2004; 91: 2649-2652. https://doi.org/10.1002/app.13445.
[56] Kang Y, Song M, Pu L, Liu T. Rheological behaviors of epoxy asphalt binder in comparison of base asphalt binder and SBS modified asphalt binder. Construction and Building Materials 2015; 76: 343-350. https://dx.doi.org/10.1016/j.conbuildmat.2014.12.020.
[57] EN 1337-3. Structural bearings Part 3: elastomeric bearings. Brussels: European Committee for Standardization 2005.
[58] ABAQUS®. Theory manual. 2014 Version 6.14.
[59] Wang Y, Liu J, Duan W, Pan Z, Qiao Y. Fatigue of vulcanized natural rubber under proportional and non-proportional loading. Fatigue & Fracture of Engineering Materials & Structures 2020; 43: 2232-2246. https://doi.org/10.1111/ffe.13250.
[60] Altalabani D, Hejazi F, Raizal Saifulnaz MR, Farah Nora Aznieta AA. Development of new rectangular rubber isolators for a tunnel-form structure subjected to seismic excitations. Structures 2021; 32: 1522-1542. https://doi.org/10.1016/j.istruc.2021.03.106.
[61] EN 1993-1-1. Eurocode 3: Design of steel structures – Part 1-1: General rules and rules for buildings. Brussels: European Committee for Standardization 2005.
[62] Kamal ZA, Arab MG, Dif A. Analysis of the arching phenomenon of bored piles in sand. Alexandria Engineering Journal 2016; 55: 2639-2645. https://dx.doi.org/10.1016/j.aej.2016.06.035.
[63] Faizi K, Armaghani DJ, Sohaei H, Rashid ASA, Nazir R. Deformation model of sand around short piles under pullout test. Measurement 2015; 63: 110-119. http://dx.doi.org/10.1016/j.measurement.2014.11.028.
[64] Li J, Tian C, Lu B, Xian Y, Wu R, Hu G, Xia R. Deformation behavior of nanoporous gold based composite in compression: A finite element analysis. Composite Structures 2019; 211: 229-235. https://doi.org/10.1016/j.compstruct.2018.12.046.
[65] Hu J, Chen W, Fan P, Gao J, Fang G, Cao Z, Peng F. Epoxy shape memory polymer (SMP): Material preparation, uniaxial tensile tests and dynamic mechanical analysis. Polymer Testing 2017; 62: 335-341. http://dx.doi.org/10.1016/j.polymertesting.2017.07.001.
[66] Kalfas KN, Mitoulis SA, Konstantinidis D. Influence of steel reinforcement on the performance of elastomeric bearings. Journal of Structural Engineering 2020: 146(10); 04020195. https://doi.org/10.1061/(ASCE)ST.1943-541X.0002710
[67] Ren X, Lu W, Zhu Y, He Y, Li T. Compressive behavior of low shape factor lead-rubber bearings: Full-scale testing and numerical modeling. Engineering Structures 2020; 209. https://doi.org/10.1016/j.engstruct.2019.110030.
[68] Potts DM, Dounias GT, Vaughan PR. Finite element analysis of the direct shear box test. Geotechnique 1987; 37 (1): 11-23.
[69] Bowles, J.E., "Foundation Analysis & Design," 5th edition, McGraw-Hill, 1996.
[70] Greco F, Luciano R, Serino G, Vaiana N. A mixed explicit–implicit time integration approach for nonlinear analysis of base-isolated structures. Annals of Solid and Structural Mechanics 2018: 10; 17-29. https://doi.org/10.1007/s12356-017-0051-z
[71] Vaiana N, Sessa S, Paradiso M, Marmo F, Rosati L. An efficient computational strategy for nonlinear time history analysis of seismically base-isolated structures. In: Carcaterra,

A., Paolone, A., Graziani, G. (eds) Proceedings of XXIV AIMETA Conference 2019. AIMETA 2019. Lecture Notes in Mechanical Engineering. Springer, Cham. https://doi.org/10.1007/978-3-030-41057-5_108

[72] Jiang Y, Zhao Z, Zhang R, Domenico DD, Pan C. Optimal design based on analytical solution for storage tank with inerter isolation system. Soil Dynamics and Earthquake Engineering 2020; 129: 105924. https://doi.org/10.1016/j.soildyn.2019.105924

[73] Mazza F, Vulcano A. Equivalent viscous damping for displacement-based seismic design of hysteretic damped braces for retrofitting framed buildings. Bulletin of Earthquake Engineering 2014; 12: 2797-2819. https://doi.org/10.1007/s10518-014-9601-5

[74] ASCE/SEI Seismic Rehabilitation Standards Committee. Seismic rehabilitation of existing buildings (ASCE/SEI 41–13). Reston, VA: American Society of Civil Engineers; 2014.

[75] ASCE. Minimum design loads for buildings and other structures. ASCE/SEI7-10. Reston, VA: American Society of Civil Engineers; 2013.

[76] Mohsenian V, Nikkhoo A, Hajirasouliha I. Estimation of seismic response parameters and capacity of irregular tunnel-form buildings. Bulletin of Earthquake Engineering 2019; 17: 5219-5239.

[77] Roy R, Thakur P, Chakroborty S. Scaling of ground motions and its implications to plan-asymmetric structures. Soil Dynamics and Earthquake Engineering 2014; 57: 46-67.

[78] Kyrkos MT, Anagnostopoulos SA. Improved earthquake resistant design of eccentric steel buildings. Soil Dynamics and Earthquake Engineering 2013: 47; 144-156. http://dx.doi.org/10.1016/j.soildyn.2012.07.011

[79] Zihms SG, Switzer C, Irvine J, Karstunen M. Effects of high temperature processes on physical properties of silica sand. Engineering Geology 2013; 164: 139-145. https://doi.org/10.1016/j.enggeo.2013.06.004

[80] Chen H, Song P, Commins T, Graham A, Trivedi AR, Siviour CR. Characterization and modelling of bisphenol-a type epoxy polymer over a wide range of rates and temperatures. Polymer 2022; 124860. https://doi.org/10.1016/j.polymer.2022.124860

[81] Ozkaya C, Akyuz U, Caner A, Dicleli M, Pinarbasi S. Development of a new rubber seismic isolator: 'Ball Rubber Bearing (BRB)'. Earthquake Engineering and Structural Dynamics 2011: 40; 1337-1352. https://doi.org/10.1002/eqe.1091

[82] Ozdemir G, Dicleli M. Effect of lead core heating on the seismic performance of bridges isolated with LRB in near-fault zones. Earthquake Engineering & Structural Dynamics 2012: 41; 1989-2007. https://doi.org/10.1002/eqe.2170

[83] Kim JH, Kim MK, Choi IK. Experimental study on seismic behavior of lead-rubber bearing considering bi-directional horizontal input motions. Engineering Structures 2019: 198; 109529. https://doi.org/10.1016/j.engstruct.2019.109529